Carbohydrate Polymers 389 (2026) 125623

Contents lists available at ScienceDirect

Carbohydrate Polymers

journal homepage: www.elsevier.com/locate/carbpol

Cationic curdlan-based hydrogels loaded with *Calendula officinalis*-decorated silver nanoparticles: Synthesis, characterization and *in vitro* biological properties

Dana M. Suflet [a,*], Irina Popescu [a], Andreea Luca [b], Maria Butnaru [b], Cristina M. Rîmbu [c], Cristina E. Horhogea [c], Marieta Constantin [a]

[a] *"Petru Poni" Institute of Macromolecular Chemistry, Grigore Ghica Voda Alley 41A, 700487, Iasi, Romania*
[b] *Faculty of Medical Bioengineering, "Grigore T. Popa" University of Medicine and Pharmacy, Str. Kogalniceanu 9-13, 700454, Iasi, Romania*
[c] *Faculty of Veterinary Medicine, "Ion Ionescu de la Brad" University of Life Sciences, Mihail Sadoveanu Alley 8, 700489, Iasi, Romania*

ARTICLE INFO

Keywords:
Cationic curdlan
Hydrogels
Silver nanoparticles
Calendula officinalis extract
Antimicrobial hydrogel

ABSTRACT

Curdlan, known for its biomedical applications, and a quaternary derivative thereof with antimicrobial properties were used to prepare new hydrogels for potential applications in wound dressings. To enhance the antimicrobial and antioxidant properties, silver nanoparticles synthesised in the presence of *Calendula officinalis*, known for its wound healing activity, were entrapped in the hydrogels. The parameters of the green synthesis of metallic nanoparticles were studied to determine the optimal conditions. Then, the spherical nanoparticles (22 nm) containing biologically active compounds from the plant extract were introduced into the cross-linking process of curdlan and quaternary derivative. The hydrogels exhibited a well-defined porous morphology (60–70 μm) with interconnected pores, which can retain up to 20.34 g/g fluid under skin-simulated conditions. The new hydrogels, with an elastic modulus between 4.85 and 11.31 kPa, exhibit complete and rapid shape recovery after progressive compression of at least five cycles. In addition, they have been shown to be biocompatible in contact with human dermal fibroblasts and can even induce their migration and proliferation within the first 8 h of contact. They have antioxidant properties and antimicrobial activity against *S. aureus* and *E. coli*, and the entrapment of silver nanoparticles leads to the augmentation of these properties.

1. Introduction

The skin, the body's largest organ, plays a crucial role in protecting against external elements, bacteria, and pathogens, while also regulating body moisture and temperature, and detecting external stimuli (Downer et al., 2023). When skin integrity is compromised, the body initiates a rapid healing response, involving the phases of hemostasis, inflammation, proliferation, and remodelling. During this stage, microorganisms can easily invade open wounds, preventing or delaying the healing process (Castano et al., 2018). Therefore, wounded skin should generally be covered with a dressing to minimise the loss of its functions and help speed up the healing process. A favourable dressing should fulfil the following characteristics: ● non-toxic, non-allergenic, and biocompatible; ● elastic, so it can easily adapt to the contours and complex shapes of wounds; ● maintain a moist environment; ● capable of absorbing exudates; ● protect the wound from bacterial infection; ● have optimal gas permeability; ● provide mechanical protection and be soft to the touch to avoid discomfort; ● easily changed and removed without causing trauma; ● able to be stored for a long time in extreme environments; ● commercially affordable; ● biodegradable (Naseri-Nosar & Ziora, 2018; Downer et al., 2023).

Hydrogel-based dressings represent one of the most advantageous approaches, as they fulfil all of the above requirements and, additionally, can incorporate various therapeutic agents that facilitate healing. Hydrogels can be prepared from synthetic, natural polymers or their mixture by various methods such as physical, chemical gelation, or self-assembly (Nasra et al., 2023; Su et al., 2021). In recent years, hydrogels obtained from natural polymers, especially polysaccharides, have been widely used due to their hydrophilicity, biocompatibility, and low toxicity (Niculescu & Grumezescu, 2022; Joshi et al., 2025).

According to the WHO (World Health Organization Newsroom, 2025), antimicrobial resistance is one of the top 10 threats to global

* Corresponding author.
E-mail address: dsuflet@icmpp.ro (D.M. Suflet).

https://doi.org/10.1016/j.carbpol.2026.125623
Received 26 March 2026; Received in revised form 24 June 2026; Accepted 3 July 2026
Available online 6 July 2026

health due to the abuse and misuse of antibiotics and the ineffectiveness of some antibacterial drugs in certain cases. Therefore, hydrogels with antimicrobial properties are extremely attractive materials for use as wound dressings (Lan et al., 2024). These hydrogels can be synthesised using: ● natural polymers with inherent antimicrobial properties, such as chitosan, alginate (Liang et al., 2024); ● polysaccharide derivatives containing hydrophobic alkyl chains and/or quaternary ammonium groups (Xia et al., 2021; Patel et al., 2024; Suflet, Popescu, et al., 2024; Wang, Zheng, et al., 2024); ● by incorporating various antimicrobial agents, such as inorganic nanoparticles, plant extracts, or drugs, to induce or enhance antimicrobial properties (Suflet, Popescu, Pelin, et al., 2021; Suflet, Constantin, et al., 2024; Li et al., 2024).

Curdlan (Curd), an extracellular polysaccharide, produced by fermentation of *Agrobacterium biobar 1* culture, with linear chains of β-(1 → 3)-D-glucan and arranged in a triple helix structure, is known to be used in the medical and pharmaceutical fields due to its immunoregulatory, anti-tumour, anti-viral, anti-inflammatory, immunomodulatory, and non-toxic properties (Majtan & Jesenak, 2018; Chen & Wang, 2020; Chaudhari et al., 2021). Moreover, curdlan derivatives containing quaternary ammonium groups have shown good antimicrobial properties against *Staphylococcus aureus* (*S. aureus)*, *Escherichia coli (E. coli)*, *Pseudomonas aeruginosa (P. aeruginosa)*, and the fungus *Fusarium* and *Candida albicans (C. albicans)* (Chen & Liang, 2017; Popescu et al., 2019). The antimicrobial activity of quaternised polysaccharides is known to be strongly dependent on both the degree of substitution and the chemical structure of the alkyl chain attached to the quaternary ammonium group. The minimum inhibitory concentration (MIC) values for quaternized curdlan derivatives have been found to range from 3 to 10 mg/mL against *E. coli*, approximately 5 mg/mL against *P. aeruginosa*, 0.5–3 mg/mL against *S. aureus*, and 0.25–2.5 mg/mL against fungal species, such as *C. albicans* and *Fusarium* spp. (Chen & Liang, 2017; Popescu et al., 2019).

Hydrogels based on curdlan and its derivatives, obtained through physical (Ding et al., 2021) or chemical (Suflet, Popescu, Prisecaru, & Pelin, 2021; Suflet, Popescu, et al., 2024; Zhang et al., 2024) cross-linking techniques, have been reported to exhibit high fluid retention capacity along with remarkable mechanical properties, being soft, flexible, and tough. Owing to their inherent biocompatibility, hemostatic properties, and antimicrobial activity, all curdlan-based hydrogels hold significant potential for applications in the medical field (Zhou et al., 2022; Ding et al., 2024; Wang, Yin, et al., 2024; Wojcik et al., 2021). Nevertheless, the potential of curdlan as a component of wound dressings has remained poorly investigated.

Inorganic nanoparticles, particularly silver nanoparticles (AgNPs), are among the most widely used nanomaterials for combating microbes, with applications across nanotechnology, bionanotechnology, medicine, industry, agriculture, and food. AgNPs can be synthesised through physical, chemical, or biological methods (Iravani et al., 2014). The biological approach offers several advantages, as it is both ecological and economical. This method consists of using microorganisms (Liu et al., 2021), algae (Chugh et al., 2021; Iravani et al., 2014) or plant extracts as reducing and capping agents of metallic nanoparticles (Dhaka et al., 2023). The use of medicinal plants in nanoparticle synthesis, known as *green synthesis*, is regarded as a clean, non-toxic, simple and cost-effective method. It is also extremely advantageous because the medicinal properties of the plants are added to the properties of the nanoparticles (Zhangabay & Berillo, 2023). In the pharmaceutical and medical industries, AgNPs are widely used owing to their broad antimicrobial spectrum, antioxidant, antifungal, anti-inflammatory, and antiviral activities (Ounkaew et al., 2020; Ounkaew et al., 2023; Sharma et al., 2009; Shrestha et al., 2024; Xu et al., 2020). The incorporation of plant extracts-capped silver nanoparticles (AgNPs) in hydrogels, films, and other biomaterial-based wound treatments has been the subject of numerous investigations. These systems' capacity to offer antimicrobial protection, promote tissue regeneration, and minimise complications related to chronic and infected wounds has made them a promising approach to wound care (Meenalotchani et al., 2025; Naseri-Nosar & Ziora, 2018).

Calendula officinalis (*C. officinalis*), belonging to the *Asteraceae* family, is a well-known medicinal plant widely used for its anti-inflammatory, antitumour, antimicrobial and wound healing activities (Sapkota & Kunwar, 2024). Chemically, *C. officinalis* contains various biologically active compounds, including carotenoids, flavonoids, terpenoids and terpenes, quinones, coumarins, phenolic acids, lipids, and polysaccharides (Sapkota & Kunwar, 2024). Recent reviews highlighted that plant-derived phytochemicals can simultaneously to initiate redox reactions that reduce silver ions (Ag^{+}) to metallic silver (Ag^{0}) (Mittal et al., 2013; Arif & Uddin, 2021). Furthermore, they can attach to silver nanoparticles through non-covalent interactions that change the free-energy order, contributing to nanoparticles' stabilisation. These phytocomponents may also provide additional antioxidant, anti-inflammatory, and regenerative effects, generating synergistic therapeutic outcomes (Oselusi et al., 2024).

A comprehensive review of the literature revealed that the incorporation of AgNPs into polymer networks based on curdlan and quaternised curdlan has not been previously reported. Furthermore, to the best of our knowledge, no studies have investigated the simultaneous use of a hydroalcoholic extract of *Calendula officinalis* as both a reducing and stabilising agent for AgNPs green-synthesis and a source of bioactive phytocomponents in the fabrication of curdlan-based hydrogels.

Therefore, the present study reports a novel strategy for the development of multifunctional hydrogels by combining the 2-hydroxypropyl-3-dimethyloctyl ammonium curdlan derivative (QCurd) and curdlan (Curd), silver nanoparticles, and a *C. officinalis* extract within a single polymeric network, aiming to formulate new materials for potential use as wound dressings. In the first step, silver nanoparticles were prepared via an eco-friendly synthesis method in the presence of a hydroalcoholic extract of *C. officinalis*. The synthesis parameters (plant extract and silver nitrate concentrations, reaction time, and temperature) were varied to determine the optimal conditions for obtaining silver nanoparticles (AgNPs-*C.off*). Taking into account the antimicrobial properties of QCurd, in the second step, a novel QCurd/Curd-based hydrogel incorporating AgNPs-*C.off* was prepared using a covalent cross-linking method. The physicochemical properties of the hydrogels were evaluated, including gel fraction, porosity, swelling behaviour under physiological conditions, X-ray diffraction patterns, and mechanical and antioxidant properties. Their biological performances, such as biocompatibility, effects on cell morphology, wound healing capacity, and antibacterial activity against *S. aureus* and *E. coli* were also assessed.

This study hypothesises that the integration of AgNPs coated with the phytotherapeutic components of *C. officinalis* extract into the network of a cationic curdlan-based hydrogel will create new materials with improved mechanical strength, antioxidant and antimicrobial properties. We anticipate that after being integrated into the curdlan network, the AgNPs to retain their potent antibacterial activity, while lowering their toxicity. In addition, the curdlan known for its wound healing ability (Chaudhari et al., 2021; Majtan & Jesenak, 2018) and the phytotherapeutic components of *C. officinalis* (Sapkota & Kunwar, 2024) could promote fibroblast migration, accelerating wound healing.

2. Materials and methods

2.1. Materials

Curdlan (Curd, $M_w \approx 1800$ kDa, determined by Gel Permeation Chromatography) was provided by Wako Pure Chemical Industries, Ltd. (Osaka, Japan). The chloride salt of 2-hydroxypropyl-3-dimethyloctyl ammonium curdlan derivative (QCurd) with a degree of substitution of 0.33 (equivalent to 1.436 meqiv. quaternary ammonium groups/g) was synthesised in our laboratory according to the method described elsewhere (Popescu et al., 2019). The pharmaceutical *C. officinalis* (*Asteraceae*) flower extract (1:5 hydroalcoholic extract, ethanol/water

= 52/48, w/w) with a solid content of 6% (*w*/w) was supplied by Dacia Plant S.R.L. (Brasov, Romania). The chemical composition of the hydroalcoholic extract of *C. officinalis* was thoroughly characterized by HPLC-ESI MS and reported elsewhere (Pelin et al., 2023). The cross-linker agent ethylene glycol diglycidyl ether (EGDGE) was achieved from Tokyo Chemical Industry (TCI), Japan, and silver nitrate ($AgNO_3$) from Honeywell Fluka (Seelze, Germany). The 2,2-diphenyl-1-picrylhydrazyl (DPPH) and 2,2′-Azino-bis-(3-ethyl)benzothiazoline-6-sulfonic acid (ABTS) were purchased from Sigma (St. Louis, MO, USA). Additionally, all experiments were conducted using deionized water.

2.2. Preparation of silver nanoparticles using C. officinalis extract

AgNPs-*C.off* were synthesised using a hydroalcoholic extract of *C. officinallis* as both reducing ($Ag^+ \rightarrow Ag^0$) and stabilising agent. To identify the optimal synthesis conditions, the influence of $AgNO_3$ concentration, *C. officinalis* extract concentration, reaction temperature and reaction time on the formation of nanoparticles was systematically investigated. Briefly, equal volumes of aqueous $AgNO_3$ solutions with different concentrations (10–60 mM) and *C. officinallis* solutions (1–10 mg/mL) prepared in ethanol:water mixture (1:1, v/v) were mixed and incubated at different temperature (25, 60, and 90 °C) under magnetic stirring (~1000 rpm) for varying times (1–8 h). The reduction of Ag^+ ions to Ag^0 was monitored by UV–vis absorption (λ = 250–850 nm) using an Evolution 201 UV spectrophotometer (Thermo Fisher Scientific Inc., USA). The AgNPs-*C.off* were recovered by centrifugation (11,000 rpm, 20 °C), washed by repeated re-dispersion/centrifugation, and freeze-dried (ALPHA 1–2 LD, Martin Christ GmbH, Germany). Reaction parameters ($AgNO_3$ concentration, *C. officinallis* extract concentration, temperature, and time) were systematically optimized to obtain nanoparticles with desired characteristics.

2.3. Preparation of QCurd/Curd hydrogels with and without AgNPs-C.off

QCurd/Curd hydrogels were prepared by mixing a 5.5% (w/w) aqueous solution of QCurd with a 5.5% (w/w) solution of Curd in 1 N NaOH at a volumetric ratio of 40:60 (Table 1) at ambient temperature, followed by the addition of the cross-linking agent (EGDGE, 18.58% (v/v)). The amount of EGDGE was calculated to achieve a molar ratio of 1:2 between the anhydroglucose units of the polysaccharides and the epoxy groups of EGDGE. Mixtures were poured into Petri dishes (d = 50 mm) or four-well cell culture plates (d = 10 mm) and maintained at room temperature for 48 h, during which the covalent cross-linking reaction of the polysaccharide chains occurred. The hydrogels were purified by repeated washing with deionized water and recovered by freeze–drying.

AgNPs-*C.off* - loaded hydrogels were prepared following the method described above with minor modifications. 0.5–3% (w/w) AgNPs-*C.off* were first dispersed by vortexing at 2000 rpm, in half of the total water volume required for QCurd dissolution, and subsequently mixed with the QCurd solution prepared in the remaining water, maintaining a final QCurd concentration of 5.5% (w/w). The AgNPs-*C.off*/QCurd mixture was gradually added to the Curd solution (5.5%, w/w), stirred briefly to homogenise, and then EGDGE was added dropwise under vigorous stirring. The procedure was then continued as described above. For all formulations, the concentration of the polymer mixtures was maintained at 5.5% (w/w), while the cross-linker content was kept constant to allow a direct comparison of the effect of AgNPs-*C.off* incorporation on the hydrogel properties.

The hydrogel samples were denoted as 40QCurd for the sample without AgNPs-*C.off* and 40QCurdAg_x for hydrogels containing green-synthesised silver nanoparticles, where "40" is the percentage of QCurd in the polysaccharide mixture (%, w/w) and *x* is the amount of AgNPs-*C.off* in the hydrogel matrix (%, w/w) (Table 1).

2.4. Characterization of silver biosynthesized nanoparticles and hydrogels

The AgNPs-*C.off* suspension was analysed by UV–Vis spectrophotometry, to measure the surface plasmon absorption (SPA).

The *shape and size* of AgNPs-*C.off* was investigated by transmission electron microscopy (TEM) using a Hitachi High-Tech HT 7700 microscope (Japan) operated in "high contrast" mode at 100 kV acceleration potential. Samples were deposited from aqueous suspension (1 mg/mL) onto 300 mesh copper grids, coated with carbon, and dried under vacuum. The size of AgNPs - *C.off* from the TEM images was analysed using ImageJ 1.48v (Wayne Rasband National Institutes of Health, USA) and OriginPro 8.5.0 (OriginLab Corporation, USA) software.

The *surface morphology* and elemental composition of AgNPs-*C.off* and hydrogels were evaluated using a Verios G4 UC Scanning Electron Microscope (SEM, Thermo Scientific, Czech Republic) equipped with an energy-dispersive spectrometer (EDS, EDAX Octane Elect Super SDD detector, USA). The samples were coated with 10 nm platinum using a Leica EM ACE200 Sputter coater to provide electrical conductivity and to prevent charge build-up during exposure to the electron beam. SEM investigations were performed in High Vacuum mode using a secondary electron detector at an accelerating voltage of 5.0 kV.

X-ray Diffraction (XRD) patterns of AgNPs-*C.off* and QCurd/Curd-based hydrogels containing AgNPs-*C.off* were performed with a Rigaku Miniflex 600 diffractometer (Rigaku, Tokyo, Japan), using CuKα-emission (λ = 1.5406 Å) in the angular range (2θ) of 10^0 to 90^0, at a scanning step of 0.01^0 and a recording rate of 5^0/min. Background subtraction, smoothing and WPPF (Whole Powder Pattern Fitting) refinement of XRD data were made using the SmartLab II v.4 software package for powder X-ray diffraction analysis, while the diffraction peaks were identified using the Crystallography Open Database (COD).

The *attenuated total reflectance Fourier Transform Infrared Spectroscopy* (ATR-FTIR) of AgNPs-*C.off* and 40QCurd hydrogels without and with nanoparticles were recorded for structural characterization using a FTIR Vertex 70 spectrometer (Bruker, Austria). The samples were examined in their solid (lyophilized) form on a KRS-5 substrate using a frequency range of 4000–400 cm^{-1}.

Silver content in AgNPs-*C.off* and hydrogels (40QCurdAg_x) was determined by atomic absorption spectroscopy (AAS). The nanoparticles and hydrogels were mineralised in 10% HNO_3 and then diluted with distilled water to a known volume. The AAS measurements were carried out in air/acetylene flame using a ContrAA 800 spectrometer (Analytik Jena, Jena, Germany).

The *porosity* (P, %) of the hydrogels was determined by the solvent immersion method (Xiang et al., 2022). The dried hydrogels with well-defined shapes were measured to determine the volume (*V*, cm^3), weighed (W_d, g), and immersed in absolute ethanol (99.5%). After 5 min

Table 1
Chemical composition and the main characteristics of 40QCurd hydrogels.

Sample code	QCurd:Curd ratio (w/w)	Ag* mg/g	GF (%, w/w)	P (%, w/w)	Pore Size** (μm)
40QCurd	40:60	–	36.4 ± 0.7	23.3 ± 1.2	62.5 ± 0.6
40QCurd$Ag_{0.5}$		$0.365 \pm 5 \times 10^{-3}$	33.8 ± 0.3	15.3 ± 0.5	74.2 ± 1.0
40QCurdAg_1		$0.99 \pm 2 \times 10^{-3}$	33.1 ± 0.7	22.7 ± 0.2	63.2 ± 1.2
40QCurdAg_3		$1.49 \pm 1 \times 10^{-3}$	33.7 ± 0.5	21.0 ± 0.9	60.5 ± 2.1

* determined by AAS.
** determined from SEM images – average pore size.

of immersion, the samples were taken out and weighed (W_s, g) after the removal of the excess alcohol. The porosity was calculated following Eq. (1):

$$P\ (\%) = (W_s - W_d)/\rho V \times 100 \quad (1)$$

where W_d and W_s represent the weight of the hydrogels before and after immersion, V is the volume of the dried hydrogels, and ρ is the density of ethanol at room temperature (0.785 g/cm^3). All experiments were performed in triplicate.

Gel fraction (GF, %) was determined to evaluate the percentage of polymer (QCurd and Curd) involved in the covalent cross-linking reaction. The *GF* can be assimilated with a degree of cross-linking (Yang et al., 2008). The hydrogels after obtaining were freeze-dried and weighed (W_i, g – the initial weight of the dry sample), then were washed with deionized water several times, when the non-cross-linked polymer chains and unreacted cross-linking agent were removed. The washed hydrogels were freeze-dried again and weighed (W_f, g – the final weight of purified sample). The gel fraction (GF, %) was calculated as:

$$GF\ (\%) = W_f/W_i \times 100 \quad (2)$$

Swelling behaviour. The ability of hydrogels to retain fluid in simulated skin conditions –phosphate buffer solution (PBS), pH = 5.5, and 32 °C – was evaluated from the swelling ratio by the gravimetric method. The dried hydrogels were weighed (W_d, g) and immersed in the PBS solution. After different time intervals, the hydrogels were withdrawn and, after careful removal of the surface solution with wet filter paper, the samples were weighed again (W_t, g). The swelling ratio (SR) was calculated using Eq. (3):

$$SR\ (\%) = (W_t - W_d)/W_d \times 100 \quad (3)$$

Mechanical Behaviour was evaluated by uniaxial compression tests of the hydrogels using a Texture Analyser (Brookfield Texture PRO CT3®, Brookfield Engineering Laboratories Inc., USA). The compression tests were performed according to the protocol described by Suflet, Constantin, et al., 2024, with slight modifications. Cylindrical hydrogel samples (18 mm diameter and 8 mm height) were previously saturated with PBS of pH 5.5 for 30 min, and then compressed until 50% deformation using a trigger load of 0.067 N at a speed rate of 0.2 mm/s. The elastic modulus (E, kPa) was calculated from the linear part of the stress–strain curves, as the slope between 5 and 20% strain. Furthermore, successive loading–unloading cyclic tests with progressive compression strain were carried out to study the reversible behaviour of the hydrogels. The hydrogels were subjected to five consecutive cyclic compressions without relaxation between each compression.

Antioxidant Activity of the *C. officinalis* extract, AgNPs-*C.off*, and the hydrogels with and without AgNPs-*C.off* was evaluated using two methods: i) the 2,2-diphenyl-1-picryl-hydrazyl (DPPH) method (Sabir et al., 2015) and ii) the 2,2′-azino-bis-(3-ethyl)benzothiazoline-6-sulfonic acid (ABTS) assay, according to the literature (Re et al., 1999).

i) *DPPH radical scavenging activity*. This method was first used to assess the DPPH free radical scavenging capacity of the plant extract. For this, 1 mL of the ethanolic solution (1:1 ethanol:water ratio, v/v) of *C. officinalis* plant extract with different concentrations (2.5 ÷ 150 μg/mL) was mixed with 0.5 mL of the ethanolic solution of DPPH (0.1 mM). The solutions were incubated for 30 min in the dark at room temperature with shaking. DPPH in its radical form (DPPH$^{\bullet}$) exhibits an absorption peak in UV–vis at a wavelength of 523 nm, which decreases with its reduction in the presence of an antioxidant compound. The DPPH scavenging effect was calculated using Eq. (4):

$$DPPH\ inhibition\ (\%) = [(A_0 - A_s) \times 100\,]/A_0 \quad (4)$$

where A_0 is the absorbance of the control sample (0,5 mL DPPH solution and 1 mL solution ethanol/water, 1:1), and A_s is the absorbance of the extract solution with DPPH. The low absorbance of the reaction mixture indicates a high DPPH free radical scavenging activity. The IC_{50}^{DPPH} value, the concentration of *C. officinalis* (μg/mL) required to reduce the initial concentration of DPPH radicals by 50%, was calculated from the graph of inhibition percentage versus *C. officinalis* concentration.

The antioxidant activity of the green-synthesised AgNPs-*C.off* and the hydrogels with and without AgNPs-*C.off* was determined by the direct contact method (Suflet, Constantin, et al., 2024). 10 mg of hydrogel or 1 mg of silver nanoparticles was immersed in 1.5 mL of DPPH ethanolic solution (0.1 mM). The solutions were shaken and incubated for different times (2, 4, 6, and 24 h) in darkness and at room temperature. The DPPH scavenging activity was determined using Eq. (4), where A_0 is the absorbance of the DPPH solution.

ii) *ABTS radical scavenging activity*. The radical scavenging activity in aqueous solution was also determined using the 2,2′-azino-bis-(3-ethyl)benzothiazoline-6-sulfonic acid (ABTS) assay, where the ABTS$^{\bullet+}$ radical cations were generated by the oxidation of ABTS with potassium persulfate (Re et al., 1999) and determined by UV–vis spectroscopy at λ = 730–740 nm. The method was slightly modified to evaluate the ABTS$^{\bullet+}$ radical cations scavenging capacity of *C. officinalis* plant extract, AgNPs-*C.off* and 40QCurd hydrogels with or without AgNPs-*C.off*. For this assay, an ABTS solution (7 mM) was mixed with $K_2S_2O_8$ solution (2.5 mM) in a volumetric ratio of 1:1 (v/v) for 16 h in the dark at room temperature before use. The ABTS$^{\bullet+}$ solution was diluted with ethanol/water 1:1 (v/v) until the absorbance value was approximately 0.7 ± 0.02 nm. Then, 1 mL of the ethanolic solution of *C. officinalis* plant extract with different concentrations (2.5 ÷ 150 μg/mL) was mixed with 0.5 mL of the diluted ABTS$^{\bullet+}$ stock solution. The solutions were incubated for 30 min in the dark at room temperature with shaking. The ABTS scavenging effect was calculated using Eq. (5):

$$ABTS^{\bullet+}\text{scavenging ability}\ (\%) = [(A_C - A_S) \times 100\,]/A_C \quad (5)$$

where A_C is the absorbance of the control sample (0,5 mL ABTS$^{\bullet+}$ with 1 mL ethanol/water 1:1, v/v), and A_S is the absorbance of the extract solution. The IC_{50}^{ABTS} value, the concentration of *C. officinalis* (μg/mL) required to reduce the initial concentration of ABTS$^{\bullet+}$ by 50%, was calculated from the graph of inhibition percentage versus *C. officinalis* concentration.

The ABTS$^{\bullet+}$ scavenging activity of the hydrogels and the green-synthesised silver nanoparticles was also determined by the direct contact method described above. 10 mg of dried hydrogel or 1 mg of silver nanoparticles was immersed in 1.5 mL of the ABTS$^{\bullet+}$ solution. The solutions were shaken and incubated for different times (2, 4, 6, and 24 h) in darkness and at room temperature. The ABTS scavenging activity was determined according to Eq. (5), but in this case, the A_C is the absorbance of the ABTS$^{\bullet+}$ stock solution.

2.5. Antimicrobial activity

Two standardized bacterial cultures of *Staphylococcus aureus* ATCC 25923 (*S. aureus*) and *Escherichia coli* ATCC 25922 (*E. coli*) were used to assess the antimicrobial activity of *C. officinalis* plant extract, AgNPs-*C. off* and the loaded and unloaded QCurd-based hydrogels with AgNPs-*C. off*.

2.5.1. MIC determination of the C. officinalis extract and AgNPs-C.off

The minimal inhibitory concentrations (MIC) were measured by the broth microdilution method (CLSI, 2012). The inocula were prepared at a final density adjusted to the 0.5 McFarland turbidity standard (10^8 colony-forming units CFU/mL). 5 mg/mL solution of hydroalcoholic extract of *C. officinalis* prepared in ethanol/water (1/1, v/v) was individually diluted with the same solvent (1/1 ethanol/water) to attain final concentrations in the range of 5 ÷ 0.0125 mg/mL. The AgNPs-*C.off* (1 mg/mL) were dispersed in sterile water to final concentrations in the

range of $1 \div 1 \times 10^{-3}$ mg/mL. Each solution (20 μL) was added to 30 μL of bacterial suspension and then inoculated with 150 μL of the broth medium (Mueller Hinton Broth, Oxford, UK), mixed with a micropipette and incubated at 37 °C for 24 h. The positive control consisted of 10 μL of bacterial culture inoculated in 190 μL of Mueller–Hinton Broth. The sterile broth medium (190 μL) represented the negative control. Bacterial growth was spectrophotometrically measured at $\lambda = 630$ nm using a Stat Fax 3200 microplate reader (Awareness Technology, USA). Two measurements were performed, before and after incubation. The lowest concentration of *C. officinalis* and AgNPs-*C.off* that inhibited the visible growth of microorganisms (MIC) was determined by fitting the maximum average absorbance values with the modified Gompertz equation (Lambert & Pearson, 2000) using GraphPad Prism 8.02 (263) software. The experiments were made in triplicate.

2.5.2. Time-kill assay

The time-elimination method was performed by distributing hydrogel samples into sterile vials containing 5 mL of bacterial suspension (1.5×10^8 CFU/mL) (CLSI, 2010). The samples were incubated for different times (6, 24, 48, and 72 h) at 37 °C. After each incubation time, the vials were vortexed at 1000 rpm for 30 s, and then 1 mL of bacterial suspension was taken out and distributed into sterile Petri dishes; the Mueller–Hinton Agar (Bio-Rad Laboratories) melted culture medium was added on top of each and cooled to 45 °C. After toughening the culture medium, the plates were incubated at 37 °C for 24 h, in a microbiological thermostat (Binder BD23, Roth, Germany), to allow the growth of the remaining viable microbial cells. After this time, all microbial colonies formed in the culture medium were counted, transformed into logarithmic values (Log_{10}) and time-kill curves were constructed by plotting Log_{10} CFU/mL against time (h). Each assay included a positive growth control (C+) represented by 1 mL of bacterial suspension with a turbidity of 0.5 McFarland standard (1.5×10^8 CFU/mL). Experiments were carried out in triplicate.

2.6. Biocompatibility

Biocompatibility tests were performed on the hydrated hydrogels cut into small pieces of 4 mm in diameter, using a biopsy punch. The material pieces were sterilized in 70% ethyl alcohol aqueous solution for 15 min, washed in sterile ultrapure water, and then equilibrated in DMEM/ F-12 cell culture medium (Gibco) for 24 h, under cell culturing conditions, at a temperature of 37 °C, CO_2 concentration of 5% and humidity of 97%.

2.6.1. MTT assay

For the MTT experiment, a fragment of pre-equilibrated hydrogel (15–16 mg) was applied over a monolayer of the normal human skin fibroblasts cell line (HDFa) with a culture surface of 1,1 cm^2 (the wells of the 48-well culture plates). Cell viability was evaluated at 24, 48 and 72 h of contact with the materials, using MTT assay protocol (Arunachalam & Sreeja, 2025). As a brief protocol, the growth culture medium from each human fibroblast culture was replaced with an equal volume (0.5 mL) of (3-[4,5-dimethylthiazol-2-yl]-2,5 diphenyl tetrazolium bromide), or MTT solution, with a concentration of 0.25 mg/mL in the culture medium without BFS. The incubation of the cells with the MTT solution for a period of 2 h took place at 37 °C, 5% CO_2, and 97% humidity. After 2 h of incubation, the MTT solution was removed and the formazan crystals formed in the cytoplasm of the cells were solubilized with an equal volume of DMSO, to that of the incubation medium. The absorbance of each formazan solution in the tested and control cultures was evaluated spectrophotometrically, using TECAN UV/VIS plate reader spectrophotometer (Tecan Sunrise, Tecan Trading AG, CH), at a wavelength of 570 nm. The percentage ratio between absorbance in experimental and control cultures was considered directly proportional to the viability of cells in experimental cultures. A minimum of three samples of each hydrogels were tested for the desired time. The results were expressed as mean and standard deviation.

2.6.2. Cell morphology evaluation

The morphology analysis of the cells in contact with the hydrogels was analysed under live culture conditions, on unstained and stained cells with the fluorescent vital dye (Calcein AM) a colourless and non-fluorescent compound, for which the cell membrane is permeable. The morphology of the HDFa cells after 72 h of cell-hydrogel interaction was analysed by incubating them for 20 min, at 37 °C, in Calcein AM solution with a final concentration of 5 μM in PBS (Phosfate Buffered Saline, Gibco) (Gilbert & Boutros, 2016). The fluorescence of hydrolysed Calcein was detected using a Leica DM IL LED Inverted Microscope with a Phase Contrast System (Leica Microsystems GmbH, Germany) at an excitation wavelength of $\lambda = 455$ nm and emission wavelength of $\lambda = 495$ nm. The cell density, cell size and cell shape were analysed on microscope captures.

2.6.3. Wound healing assay

The wound healing assay was performed according to an existing protocol in which cell migration was followed at different time intervals (Jonkman et al., 2014). For this, a 48-well plate was prepared by culturing 1×10^4 HDFa cells/well in DMEM/F-12 medium until a confluent monolayer of cells was obtained. Using a 200 μL pipette tip, a scratch was made in each of the tested wells. The detached cells were removed by washing the wells twice with culture media. To obtain consistent results without a mechanical influence of the materials on the cells, material extracts were used for testing. For this, 50 mg of each material (cut into equal fragments of 15–16 mg each) were incubated in 5 mL of culture medium for 72 h, at 37 °C. The extraction medium was used for the wound healing-healing assay, adding 0.5 mL to each scratched wells. Each extract was tested in triplicate. The migration of the cells into the gap was observed at different time intervals (0, 4, 8, and 24 h) after staining with BioTrackerTM Green CSFE Cell Proliferation kit, according to the manufacturer's protocol, using an inverted fluorescence microscope (Leica DM IL), for the tested materials and the control. The images were analysed using ImageJ software with the Wound_Healing_Size_Tool Plugin.

2.6.4. Statistical analysis

The results are expressed as mean - standard deviation (SD). Statistical differences between groups were analysed using one-way ANOVA followed by *t*-Test (Two-Sample Assuming Equal Variances).

3. Results and discussion

3.1. Preparation and characterization of silver nanoparticles using *Calendula officinalis*

Plant-derived biomolecules (phytochemicals) such as phenolic compounds, terpenoids, carbohydrates, and flavones are known to act as reducing agents in the green-synthesis of metallic nanoparticles (Arif & Uddin, 2021; Mittal et al., 2013). These biomolecules effectively reduce Ag^+ to Ag^0, acting simultaneously as both a reducing and a stabilising agent. Furthermore, the resulting AgNPs are expected to be enriched with the intrinsic medicinal properties of plant extract. Specifically, we used the hydroalcoholic extract of marigold (*Calendula officinalis*) as a reducing agent. This extract is widely used in the Romanian pharmaceutical industry due to its unique benefits in supporting normal liver function. There are numerous reports on the synthesis of AgNPs using aqueous extracts of *C. officinalis* (Baghizadeh et al., 2015; Santos et al., 2022; Sapkota & Kunwar, 2024); however, the hydroalcoholic extract has never been investigated as a reducing agent. By using it, we expect that AgNPs will be incorporated into a matrix that includes both hydrophilic and hydrophobic components of *C. officinalis*.

The optimal conditions for obtaining stabilised AgNPs in the presence of *C. officinalis* were first investigated. Thus, different

concentrations of $AgNO_3$ (10–60 mM) were mixed with a hydroalcoholic solution of *C. officinalis* of fixed concentration (1 mg/mL) for 3 h at 60 °C. The reaction kinetics were monitored by UV–Vis absorption spectroscopy in the visible range (250–900 nm), where silver nanoparticles typically exhibit the characteristic surface plasmon resonance (SPR) band arising from free electron excitation.

The plasmon absorption of AgNPs-*C.off* was observed at λ = 434–480 nm (Fig. 1a). Increasing the $AgNO_3$ concentration from 10 to 40 mM led to an increase in the maximum absorption at 434 nm, while further increase to 50 and 60 mM caused both a shift of the absorption maximum to longer wavelengths (472–480 nm) and a decrease in the adsorption maximum, which can be attributed to the agglomeration of nanoparticles (He et al., 2017). Fig. 1b shows the variation of the UV–Vis absorbance of the silver nanoparticles synthesised in the presence of *C. officinalis* plant extract (1 mg/mL) for 1 h and 3 h, using 40 mM $AgNO_3$ at different temperatures. The curve shape and the high absorption peak intensity of AgNPs synthesised at 60 °C for 3 h indicate the formation of small and uniformly distributed nanoparticles. By contrast, increasing the reaction temperature to 90 °C resulted in a strong tendency towards nanoparticle agglomeration after 3 h, leading to the disappearance of the absorption maximum. The synthesis of small-sized AgNPs, but in smaller quantities, at a shorter reaction time (1 h) is indicated by the intensity peak at 400 nm. Similar trends have been reported in the literature for AgNPs synthesised in the presence of polysaccharides (e.g., oxidised pullulan) (Constantin et al., 2023), algae (Prasad et al., 2013), and plant extracts (Ansari et al., 2023).

As is known, reaction time is a key factor influencing the formation of nanoparticles in biosynthesis techniques. In the present study, the optimal reaction time was found to be 3 h (Fig. 1c). The influence of the *C. officinalis* extract concentration on the biosynthesis of AgNPs was also investigated (Fig. 1d). The experiment was conducted using 40 mM $AgNO_3$ and varying the extract plant concentration (1–10 mg/mL). Results showed that increasing the extract concentration promoted the formation of more and larger AgNPs, as evidenced by the maximum absorbance intensity shifting to higher wavelengths (435 → 487 nm), due to the increase in the hydrophobic part covering the nanoparticles. In order to keep a good dispersibility and small size of AgNPs-*C.off,* 1 mg/mL was selected as the best plant extract concentration for the synthesis of nanoparticles. Based on these results, the optimal parameters for the preparation of AgNPs-*C.off* were chosen, namely: 40 mM the concentration of aqueous solution of $AgNO_3$, 1 mg/mL the concentration of hydroalcoholic *C. officinalis* extract plant, the reaction time of 3 h, and 60 °C temperature. The nanoparticles were purified to remove the residual ions (Ag^+ and NO_3^-) by centrifugation (20 °C and 11,000 rpm) followed by re-dispersion in distilled water. This washing process was repeated three times.

The size and morphology of the biosynthesized nanoparticles were evidenced by electronic microscopy (TEM and SEM). TEM images

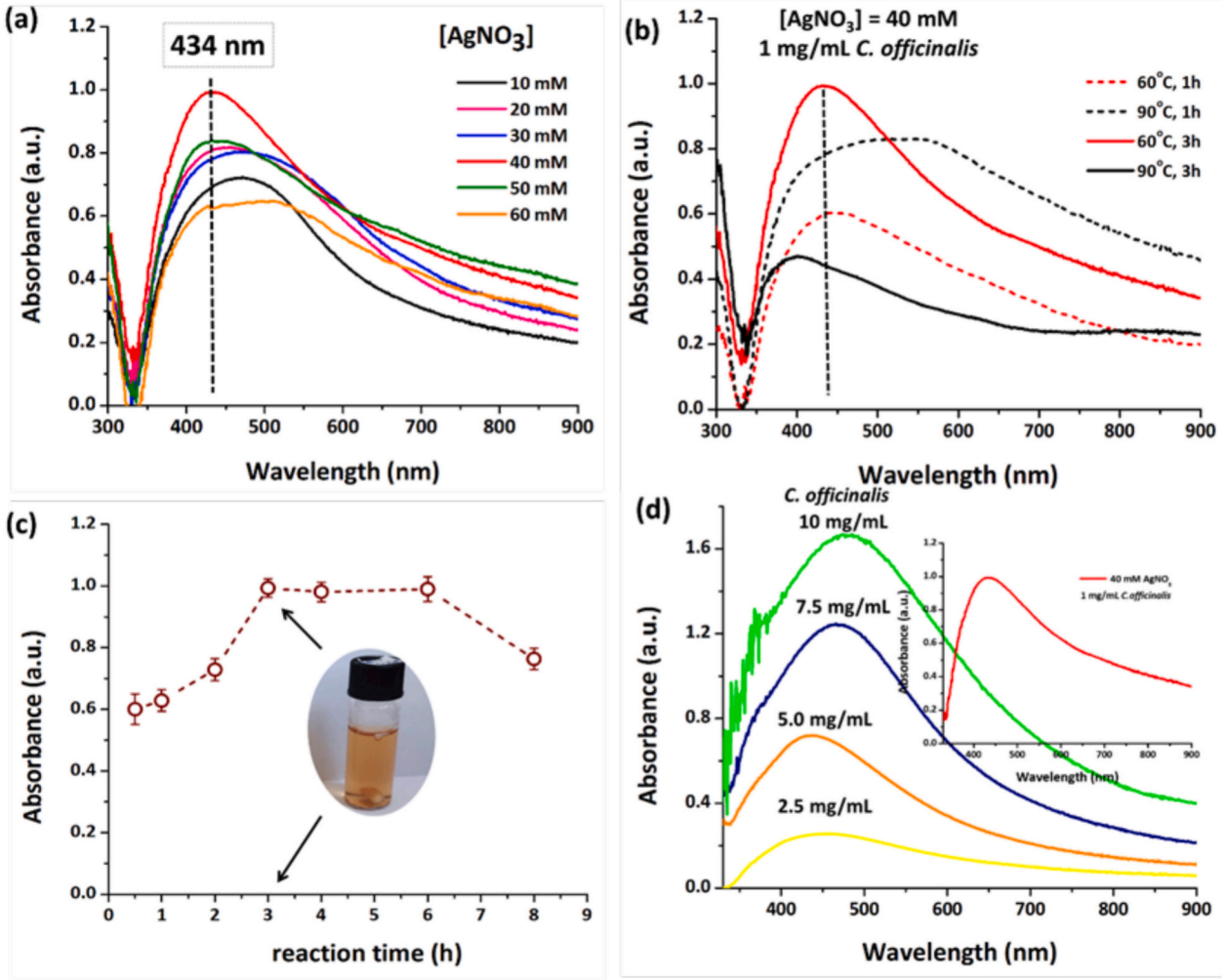

Fig. 1. UV–Vis spectra of AgNPs prepared in different conditions using *C. officinalis* as reducing agent at different: (a) concentrations of $AgNO_3$ ([*C. officinalis*] = 1 mg/mL, 60 °C, 3 h); (b) reaction temperatures ([$AgNO_3$] = 40 mM, [*C. officinalis*] = 1 mg/mL); (c) reaction times ([$AgNO_3$] = 40 mM, [*C. officinalis*] = 1 mg/mL, 60 °C); (d) concentrations of *C. officinalis* extract ([$AgNO_3$] = 40 mM, 60 °C (UV spectra for 5-fold diluted reaction solution; insert picture: without dilution).

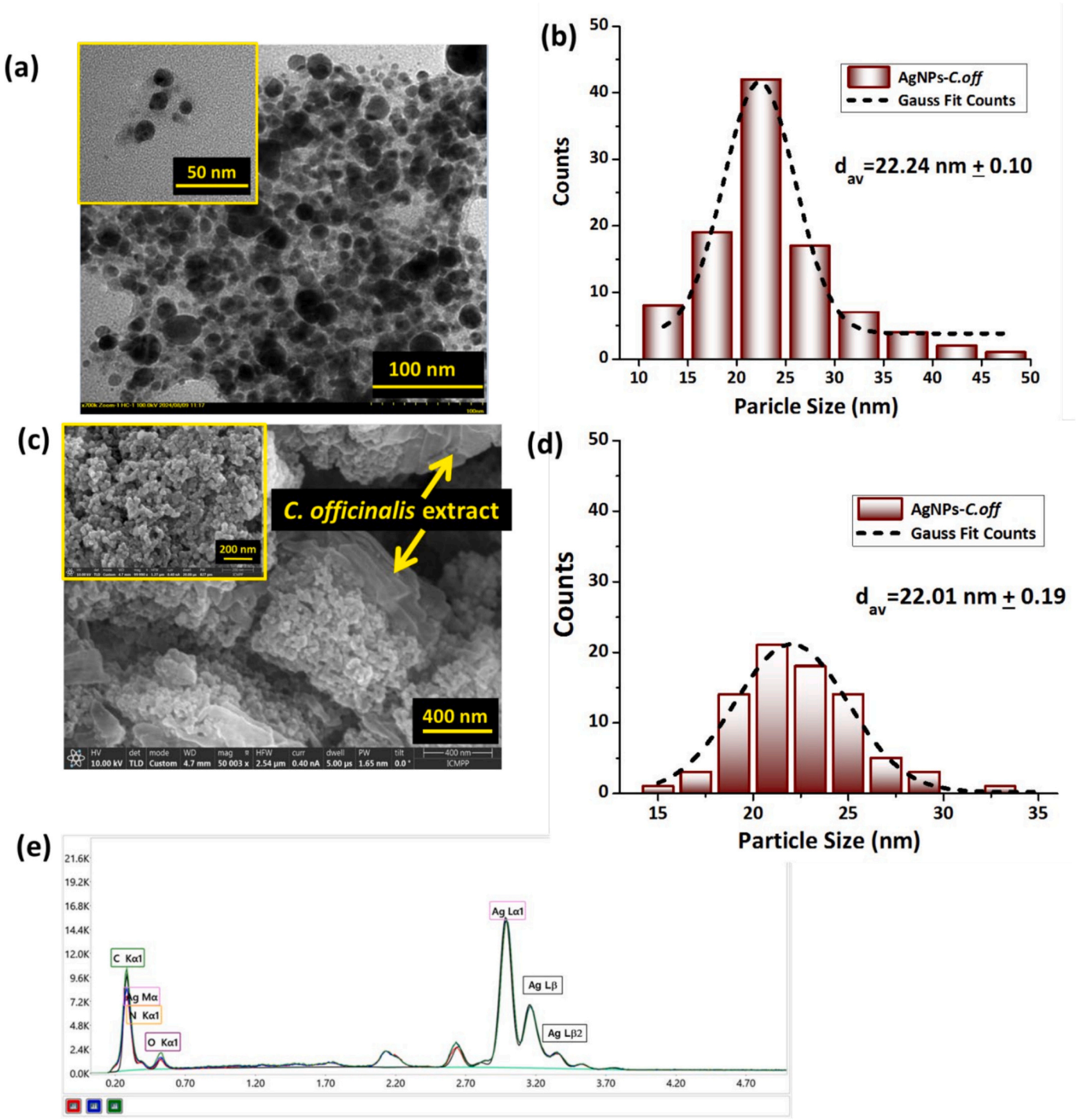

Fig. 2. Electronic microscopy of AgNPs-*C.off*: TEM images (a) and SEM microphotographs (c); (insert: detailed TEM and SEM images); size histograms from TEM (b) and SEM (d); SEM-EDX analyses of AgNPs-*C.off* (e).

(Fig. 2a) revealed uniformly distributed and spherical nanoparticles with an average size of 22.24 ± 0.10 nm (Fig. 2b). The presence of small aggregates and coating of nanoparticles by organic components from the extract was also observed. The SEM micrographs confirmed the formation of uniform and spherical nanoparticles with sizes ranging from 15 to 35 nm (the average size: 22.01 ± 0.19 nm) (Fig. 3c, d). In addition, the organization of nanoparticles into aggregates, including the organic substrate of the extract, was also highlighted. The EDX analyses of AgNPs-*C.off* (Fig. 3e) showed signals of varying intensities along the X-axis at different binding energies (keV), indicating the presence of several elements in the sample. The strong absorption signals at approximately 3 and 3.2 keV confirmed the presence of nanocrystalline metallic silver in the green-synthesised nanoparticles, attributable to surface plasmon resonance (Jagtap & Bapat, 2013). Carbon and oxygen were also detected in the spectrum, corresponding to organic compounds from the *C. officinalis* extract, either adsorbed on the surface of AgNPs-*C.off* or incorporated within the nanoparticle aggregates, which play a crucial role in the reduction, stabilisation, and biological properties of biosynthesized silver nanoparticles (He et al., 2017).

The silver content of AgNPs-*C.off* determined by atomic absorption spectroscopy (AAS), confirmed the presence of metallic silver at a ratio of 103.9 ± 2.45 mg Ag^0 per gram of AgNPs-*C.off*.

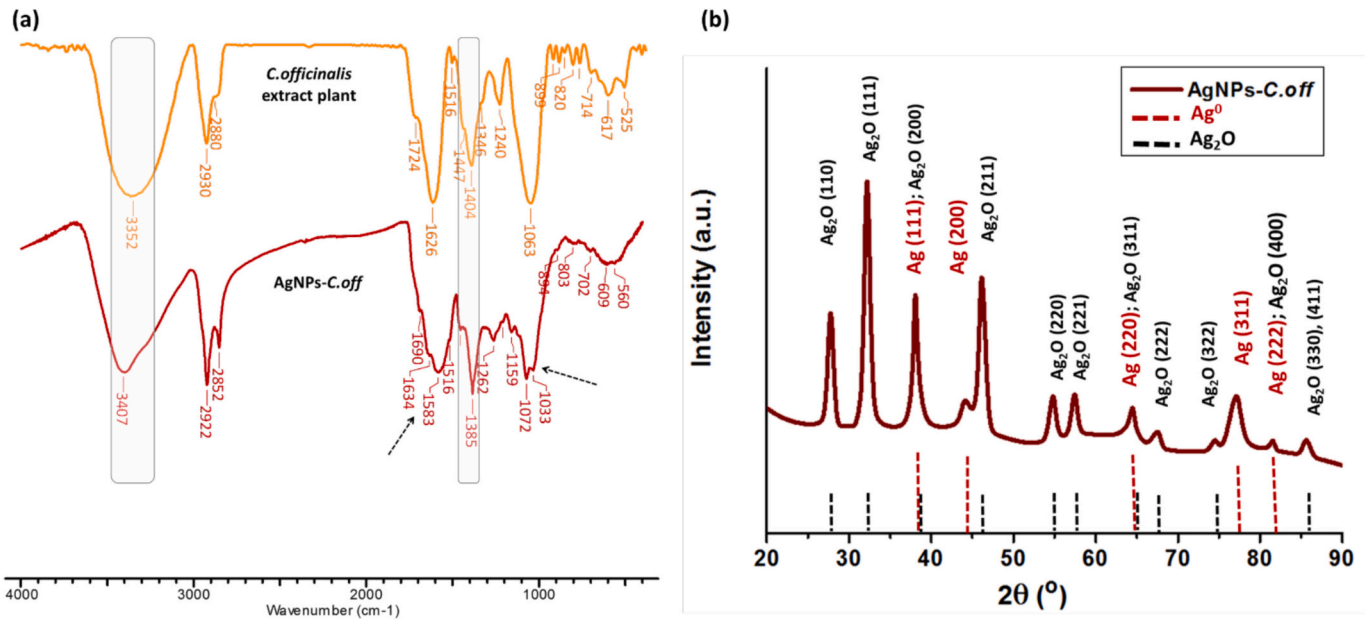

Fig. 3. ATR-FTIR spectra of the *C. officinalis* extract and the green-synthesised silver nanoparticles (a); X-ray diffraction spectrum of AgNPs-*C.off* (b).

The reducing and stabilising role of the extract in the synthesis of AgNps-*C.off* was further proved by ATR-FTIR and X-ray spectrometry (Fig. 3).

FT-IR analysis of *C. officinalis* extract (Fig. 3a) presents characteristic peaks as: stretching vibration of O—H groups and hydrogen bonds (3352 cm^{-1}) characteristic of polyphenolic compounds; asymmetric and symmetric C—H stretching from aliphatic groups (2930 and 2880 cm^{-1}); C═O stretching from carbonyl and carboxylic groups (1724 cm^{-1}; 1626 cm^{-1}); C=C–C stretching from aromatic and olefinic compounds (1516 cm^{-1}, 1447 cm^{-1}); C–O–H deformation of phenols from flavonoids (1404–1346 cm^{-1}); C—O, C—H stretching from phenolic and ether groups of monosaccharide units in the branched regions and flavonoids (1240 cm^{-1}); and C_{ar}–O–C_{al}, C—O groups of carbohydrate monomers (1063 cm^{-1}). Out-of-plane bending bands of aromatic C—H were observed at 899–525 cm^{-1} (Hemlata et al., 2020; Pelin et al., 2023; Sapkota & Kunwar, 2024).

The formation of AgNPs-*C.off* was confirmed by the presence of the characteristic signals of the extract, and the slight shifts of the bands at 3407 and 1385 cm^{-1} towards higher or lower wavelengths indicated the interaction between silver and the phytocomponents of the extract, which act simultaneously as reducing, capping, and stabilising agents. In addition, the splitting of the main bands at 1626 cm^{-1} and 1063 cm^{-1}, with the highlighting of the characteristic bands –COO^-, C—O and H—O, could be due to both the oxidation of the phytopharmaceutical compounds (Sapkota & Kunwar, 2024) and the breaking of hydrogen bonds with the formation of new coordination bonds with the silver atom.

The crystalline structure of AgNPs-*C.off* was confirmed by X-ray diffraction (XRD) analysis. Fig. 3b shows diffraction peaks at $2\Theta = 38.03^0$, 44.02^0, 64.47^0, 77.09^0, and 81.57^0 corresponding to the (111), (200), (220), (311), and (222) crystalline planes of face-centered cubic (fcc) metallic silver (space group 225:Fm-3 m, Card No. 9011607). Because these nanoparticles were synthesised in the presence of a plant extract, some components of the extract were highly sensitive and prone to oxidation. Thus, the spectrum revealed the presence of Ag_2O nanoparticles formed by the reaction of Ag^+ with components from *C. officinalis* extract. Diffraction peaks at $2\Theta = 27.72^0$, 32.17^0, 38.03^0, 46.07^0, 54.79^0, 57.42^0, 64.47^0, 67.54^0, 74.49^0, and 82.5^0 correspond to the (110), (111), (200), (211), (220), (221), (311), (222), (332), (400), (411), and (330) planes of Ag_2O nanoparticles (space group 201:Pn-3:1, Card No. 1010604) (He et al., 2017; Santos et al., 2022; Patel & Joshi, 2023). These results were further supported by energy dispersive X-ray spectroscopy (EDX) (Fig. 2e), which confirmed the presence of C, O, N, and Ag attributed to the AgNPs-*C.off* and the platinum coating layer.

3.2. Synthesis and characterization of 40QCurd hydrogels with and without AgNPs-C.off

The new matrix for embedding AgNPs-*C.off* was prepared from QCurd and Curd through a covalent cross-linking technique, using EGDGE as the cross-linking agent. The reaction was carried out at ambient temperature in alkaline medium. Based on our previous studies on hydrogels based on curdlan and its quaternary derivatives (Suflet, Popescu, et al., 2024), an optimal ratio of 40:60 (*w*/w) between QCurd and Curd was selected. Table 1 summarizes the main properties of the newly synthesised hydrogels, both without and with incorporated silver nanoparticles, while Scheme 1 illustrates the chemical structure of the hydrogel components and provides a schematic representation of the preparation process.

3.2.1. Gel fraction

The gel fraction (GF, %) is a key parameter in hydrogel characterization, representing a measure for quantifying the cross-linking density efficiency of polysaccharide hydrogels. Analysis of the GF data (Table 1) indicated that the presence of silver nanoparticles did not significantly influence the cross-linking degree. The GF value was determined to be 36.4% for the hydrogel without silver nanoparticles, and between 33.1 and 33.8% for the composite hydrogels. The relatively low GF values can be attributed to the limited accessibility of the cross-linker agent to hydroxyl groups, as a result of the reduced flexibility of the EGDGE structure due to the short length of the aliphatic chain between the epoxy groups (approximately 19.14 Å, Nenitescu, 1966). Additionally, amphiphilic polymers are known to self-organize into hydrophobic micro-domains or vesicular aggregates in aqueous environments of about 5 μm, which can also obstruct the cross-linking reaction of polysaccharide chains (Hatano et al., 2016; Suflet, Popescu, et al., 2024). The slight decrease in GF values for hydrogels with silver nanoparticles can be attributed to the coordinative bonds between Ag^0 atoms and OH groups, which block the cross-linking sites (Scheme 1). As GF values show (Table 1), increasing the amount of AgNPs-*C.off* in hydrogels did not significantly influence the degree of cross-linking of the hydrogels.

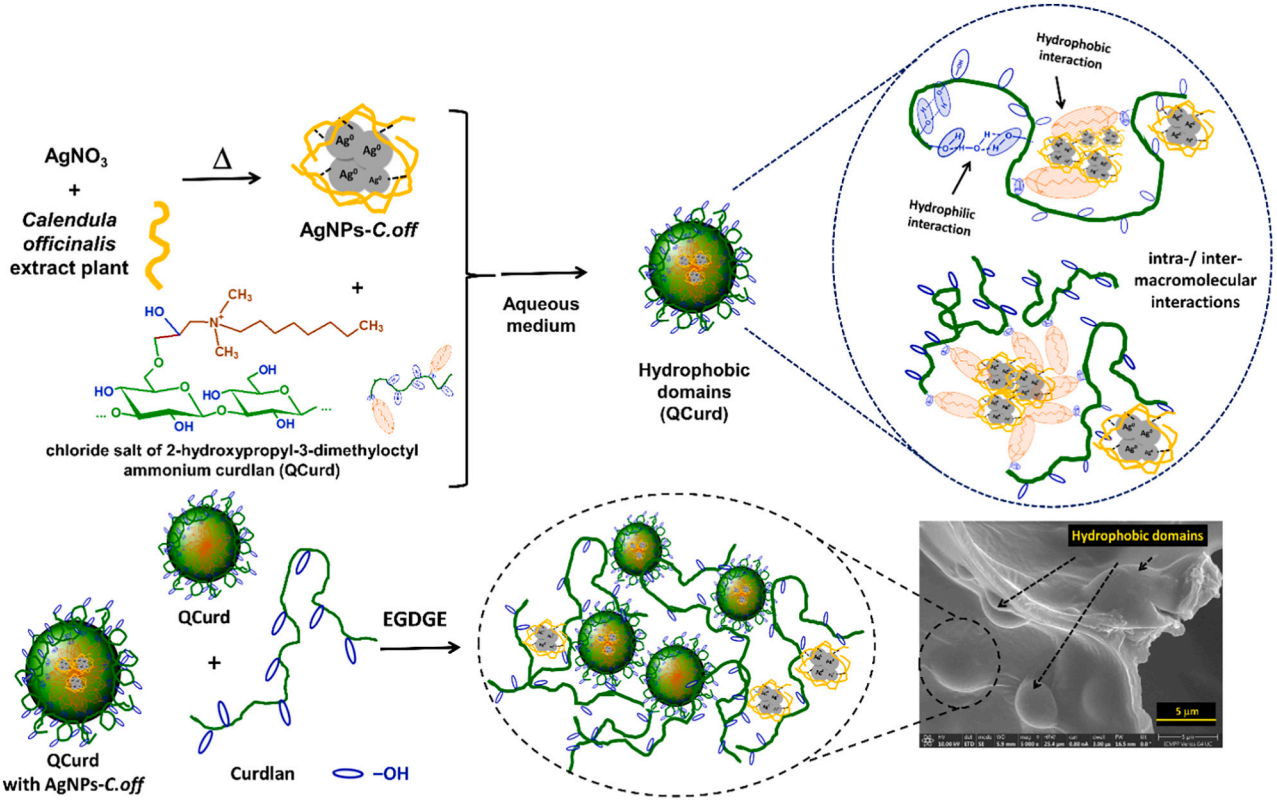

Scheme 1. Schematic representation of the preparation of AgNPs-*C.off* and AgNPs-*C.off* loaded-40QCurd hydrogel

3.2.2. Morphology and pore size

As result of chemical cross-linking, a tree-dimensional network with a uniform pore distribution was observed in the cross-sectional scanning electron micrographs of the hydrogels (Fig. 4). Moreover, the SEM images highlight the presence of hydrophobic domains along the pore walls, generated by rearrangement of octyl chains from the quaternary ammonium groups of the QCurd derivative during the dissolution process (Scheme 1). The hydrogel without AgNPs-*C.off* (40QCurd) shows pores with an average size of 62.5 ± 0.6 µm and a uniform, narrow distribution (Table 1, Fig. S1). The presence of silver nanoparticles slightly influenced the pore size and distribution. Incorporation of AgNPs-*C.off* led to a slight increase in pore size and widening of the pore distribution. This behaviour could be explained by the partial hindrance of the cross-linking process caused by hydrophobic compounds present in the plant extract, as also reflected by the decrease in GF (Suflet, Popescu, et al., 2024). In addition, SEM-EDX images of the hydrogels surfaces (Fig. 4b, Fig. S1c) confirmed the presence of Ag atoms, showing a uniform distribution of silver throughout the hydrogel matrix.

To evidence the interactions between the polymeric matrix and the phytocomponents of *C. officinalis* extract covering AgNPs, the ATR-FTIR spectra of the unloaded (40QCurd) and AgNPs- *C.off* - loaded (40QCurdAg$_x$) hydrogels are compared in Fig. 5a-c. The bands observed for AgNPs-*C.off* - loaded hydrogels were almost superimposable to those of the sample without metal nanoparticles. However, by adding AgNPs-*C.off*, due to the contribution of the plant extract, an intensification of the large O—H band at 3400 cm^{-1} and of the C—O stretching vibrations

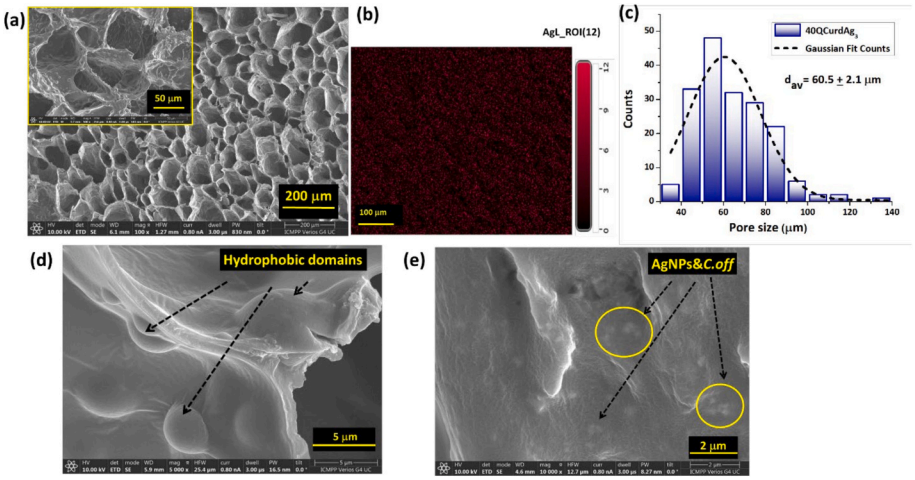

Fig. 4. SEM micrographs of the hydrogel with AgNPs-*C.off* (40QCurdAg$_3$): cross section (a); the mapping image for Ag (b); size pore distribution diagram (c); hydrophobic micro-domains in the pore wells (d); the AgNPs-*C.off* presence in the hydrogel structure (e).

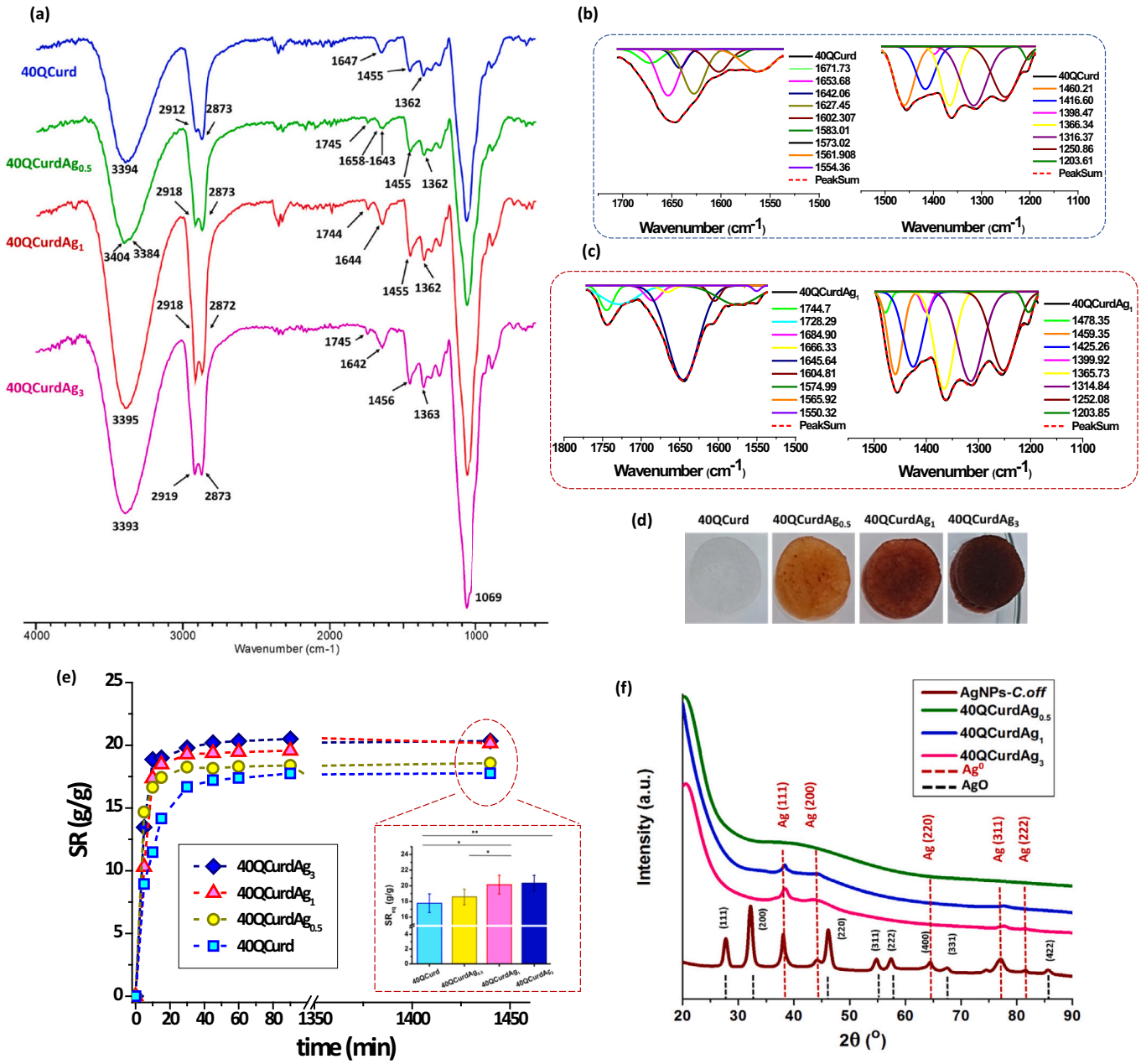

Fig. 5. ATR-FTIR spectra of hydrogels without and with AgNPs-*C.off* (a); the deconvolution of the bands at 1800–1550 cm^{-1} and 1500–1200 cm^{-1} from the ATR-FTIR spectrum of 40QCurd hydrogel (b) and 40QCurdAg$_1$ (c); optical images of hydrogels without and with AgNPs-*C.off* in the swollen state (d); swelling kinetics in PBS solutions with pH 5.5 at 32 °C and the equilibrium swelling ratios at 24 h (e); XRD patterns of composite 40QCurd-based hydrogels and AgNPs-*C.off* (for comparison) (f).

at 1069 and 1043 cm^{-1}, associated with both curdlan and phenolic compounds, occurs (Fig. 5a). Higher AgNPs-*C.off* content gradually increases the strength of these bands, indicating an increase in hydrogen bonding interactions and short-range physicochemical crosslinking between phytochemicals and the curdlan network (Usme-Duque et al., 2026). By strengthening the hydrogel network through multiple hydrogen-bonding crosslinking interactions, these interactions may help explain the morphology changes observed (Fig. 4) and the enhanced water retention capacity (Fig. 5c).

The slight shift in the asymmetric CH_2 stretching vibrations of the alkyl chains at 2912 cm^{-1} in 40Qcurd to 2018–2019 cm^{-1} in the loaded hydrogels, along with the increase in the intensity in the region 3000–2800 cm^{-1}, can reflect a strong hydrophobic interaction of these groups with aromatic components of plant extract (Coates, 2000). The peak at 1745 cm^{-1}, attributable to an ester C═O stretching vibration associated with esterified carotenoid profile of the marigold flower (Mukhtar et al., 2004) appears more intense as the AgNPs-*C.off* amount increases, especially in 40QCurdAg$_1$. This indicates that phenolic compounds may serve as crosslinking mediators, increasing the density of the polymeric network by extra hydrogen bonding and potentially π–π stacking interactions. The band at 1684.9 cm^{-1} (deconvoluted 1700–1500 cm^{-1} spectrum region) in 40QCurdAg1 (Fig. 5c) can be assigned to intermolecular H-bonding of aromatic esters (C=O) in the *C. officinalis* extract with OH functionalities of polymeric matrix (Pelin et al., 2023).

Additionally, the bands at 1666.3 cm^{-1} and 1604.8 cm^{-1} (Fig. 5c) can be attributed to the aromatic C═C stretching or conjugated carbonyl groups in terpenoids and flavonoids present in the flower extract, which are involved in interactions with the functional groups of the matrix (Kozlowska et al., 2018). In this region, C—H bending vibrations in

quaternary ammonium salts (1460.2 cm^{-1} in 40QCurd) involved in the interaction with plant extract components were linked to a new peak at 1478.3 cm^{-1} in the AgNPs-*C.off* - loaded hydrogels. Also, the blue shift of C—N stretching vibration from the quaternary ammonium groups of QCurd from 1416.6 to 1425.2 cm^{-1} in 40QcurdAg$_1$ hydrogels indicates changes in the conformational structures within the alkyl chains attached to the nitrogen atom. All these observations constitute evidence for the presence of the plant extract-AgNPs in hydrogels, suggesting that its components were associated via H-bonds (involving the OH groups of phenols and the C═O of the C-ring) (Batain et al., 2020; Catauro et al., 2020) and hydrophobic interactions with the octyl chains of quaternary ammonium groups of QCurd (aromatic ring).

3.2.3. Swelling behaviour

Considering the intended application, the swelling behaviour of the hydrogels was evaluated under physiological conditions simulating the skin environment (pH 5.5 and 32 °C). Under these conditions, the swelling will be a result of the balance between the hydrophilic charged quaternary nitrogen of QCurd and the hydrophobic interactions generated by the octyl chains of the curdlan derivative, together with the hydrogen bonds between curdlan chains, or curdlan chains and *C. officinalis* plant extract components. Fig. 5d shows the optical images of hydrogels without and with AgNPs-*C.off* in the swollen state, where changes from light to dark brown colour can be observed with increasing AgNPs-*C.off* content. The swelling behaviour revealed rapid swelling kinetics, with equilibrium reached within the first 30 min (Fig. 5e), characteristic of lyophilized hydrogels with large pores. Thus, an equilibrium swelling ratio (SR_{eq}) of 17.77 $g_{PBS}/g_{hydrogel}$ was obtained for the 40QCurd sample that increased slightly with the addition of AgNPs-*C.off* to 18.58, 20.13, and 20.34 g/g for 40QCurdAg$_{0.5}$, 40QCurdAg$_1$, and 40QCurdAg$_3$, respectively. This behaviour may be attributed to the presence of soluble phytocomponents from *C. officinalis* extract and, at the same time, to the interconnected porous structure and the hydrophilic-hydrophobic balance of the curdlan/quaternary curdlan network, which can modify water distribution and hydration dynamics within the matrix, thereby facilitating higher water uptake (Tak et al., 2023). The water absorption of all 40Qcurd hydrogels, without or with AgNPs/*C.off* ranged between 17 and 20 g/g, indicating the ability of the composite materials to absorb liquids weighing more than 17 times the dry weight of the sample. These swelling ratios are consistent with other polysaccharide-based hydrogels proposed as wound dressings, such as chitosan, alginate, cellulose and curdlan-derived hydrogels, placing them in the category of high-swelling hydrogels with applications in wound healing and tissue regeneration (Feng & Wang, 2023). Moreover, the water absorption capacity of 40QCurdAg hydrogels is close to that reported for commercial wound dressings based on ionic polysaccharides like alginate or carboxymethylcellulose, which have swelling ratios between 15 and 23 g/g (Minsart et al., 2022; Parikh et al., 2011), suggesting that the obtained composite hydrogels, in terms of swelling, are suitable for managing infected or highly exuding wounds. Therefore, the swelling capacity observed in the present study appears to be particularly advantageous for biomedical applications, especially in wound dressings, where rapid adsorption and retention of wound exudate are essential for maintaining a moist healing environment and promoting tissue regeneration.

3.2.4. XRD analysis

XRD analyses were performed to evidence the presence of *AgNPs-C. off* within the hydrogel structure, distinguishing whether they were only surface-exposed or embedded/coated within the polysaccharide network (Fig. 5f). In the case of the 40QCurdAg$_{0.5}$ hydrogel, the XRD spectrum did not display the characteristic diffraction peaks of metallic silver (Ag^0). This absence can be attributed to the low AgNPs-*C.off* amount, as well as their complete encapsulation by hydrophobic domains and polysaccharide chains of QCurd and Curd.

Increasing the AgNPs-*C.off* content allowed the most intense Ag^0 peaks at $2\Theta = 38.03^0$, 44.02^0, and 77.09^0 ((111), (200), and (311) planes) to appear. These results support the assumption that silver nanoparticles were encapsulated both the hydrophobic and hydrophilic domains of the polysaccharide chains of QCurd and Curd, as illustrated in Scheme 1. If the nanoparticles had been exposed on the hydrogel surface, the XRD spectrum would have exhibited the specific Ag^0 peaks regardless of their quantity, as reported in the literature (Suflet, Popescu, Pelin, et al., 2021).

The final amount of silver in AgNPs-*C.off*-loaded 40QCurd hydrogels (Table 1), as determined by AAS, was in good agreement with the initial amount of silver used in the hydrogel preparation process. This supports the hypothesis that AgNPs are trapped between the polysaccharide chains and are not released during washing step of the hydrogels.

3.2.5. Mechanical properties

The compressive strength (σ, kPa) of QCurd/Curd-based hydrogels is a critical mechanical property for specific biomedical applications, particularly for wound dressings. Fig. 6 presents the uniaxial compression curves, performed on the hydrated hydrogels in simulated skin physiological medium (PBS, pH = 5.5). All samples were subjected to progressive compression up to 50% strain (Fig. 6a), where they demonstrated resistance without fracture, indicating good compressive strength. It is known that the mechanical properties of hydrogels are influenced by their chemical structure and morphology (e.g. pore size and distribution, cross-linking density). The lowest mechanical characteristics (E = 4.85 kPa, σ_{50} = 10.52 kPa) were displayed by the sample without silver nanoparticles (40QCurd). The elastic modulus values are close to those reported in the literature for QCurd-based hydrogels cross-linked with 1,4-butanediol diglycidyl ether (E = 7.8 kPa, σ_{ut} = 18 kPa) (Suflet, Popescu, et al., 2024). The incorporation of silver nanoparticles into the hydrogel matrix exerted a slight reinforcing effect, evidenced by an increase in the strength force at 50% compression (σ_{50}, kPa) and elastic modulus (10.54 kPa for 40QCurdAg$_{0.5}$, and 11.31 kPa for 40QCurdAg$_1$). This increase is due to the interaction between AgNPs-*C. off* and polymeric matrix by creating more hydrogen bonds. However, a higher AgNPs-*C.off* content (40QCurdAg$_3$) leads to a decrease in the elastic modulus to 6.67 kPa. This behaviour could be attributed to AgNPs-*C.off*, which, when added in large quantities into the polymer network during the cross-linking can block the access of the cross-linking agent to the OH groups of polymers, as confirmed by its similar physicochemical properties with 40QCurdAg$_1$ (Table 1, Fig. 6b) and FT-IR analysis (Fig. 5a). Moreover, the phenolic compounds can interact non-covalently with polysaccharides that have numerous hydroxyl functions, especially through hydrogen bonds and hydrophobic associations (Le Bourvellec & Renard, 2012). These interactions could reduce the effective crosslink density by competitively interfering with polymer-polymer associations.

The strain-stress curves of the hydrogels exhibited profiles characteristic of viscoelastic materials, which dissipate energy during deformation, as evidenced by the hysteresis observed in the loading-unloading curves (Fig. 6a insert). The dissipation energy (kJ/m^3) corresponds to the hysteresis area between the loading and unloading curves. As a consequence of this dissipation, the loading and unloading responses are not always identical, being dependent on the internal structure of the hydrogel. A summary of the main mechanical characteristics is listed in Table 2.

The progressive increase in compressive strain from 30 to 50% (Fig. 6b) shows an ideal viscoelastic behaviour of the hydrogels, as evidenced by the good overlap of the loading curves. Moreover, the compression tests with five consecutive loading-unloading cycles (Fig. 6c, Fig. S2), performed at the same strain without relaxation time, did not significantly influence the mechanical behaviour, as reflected by the hysteresis curves. Also, no noticeable cracking or structural damage was observed after five cycles at a strain of 50%, indicating that the hydrogels exhibit excellent recoverability. According to the literature, the closed loading–unloading curves with pronounced hysteresis loop

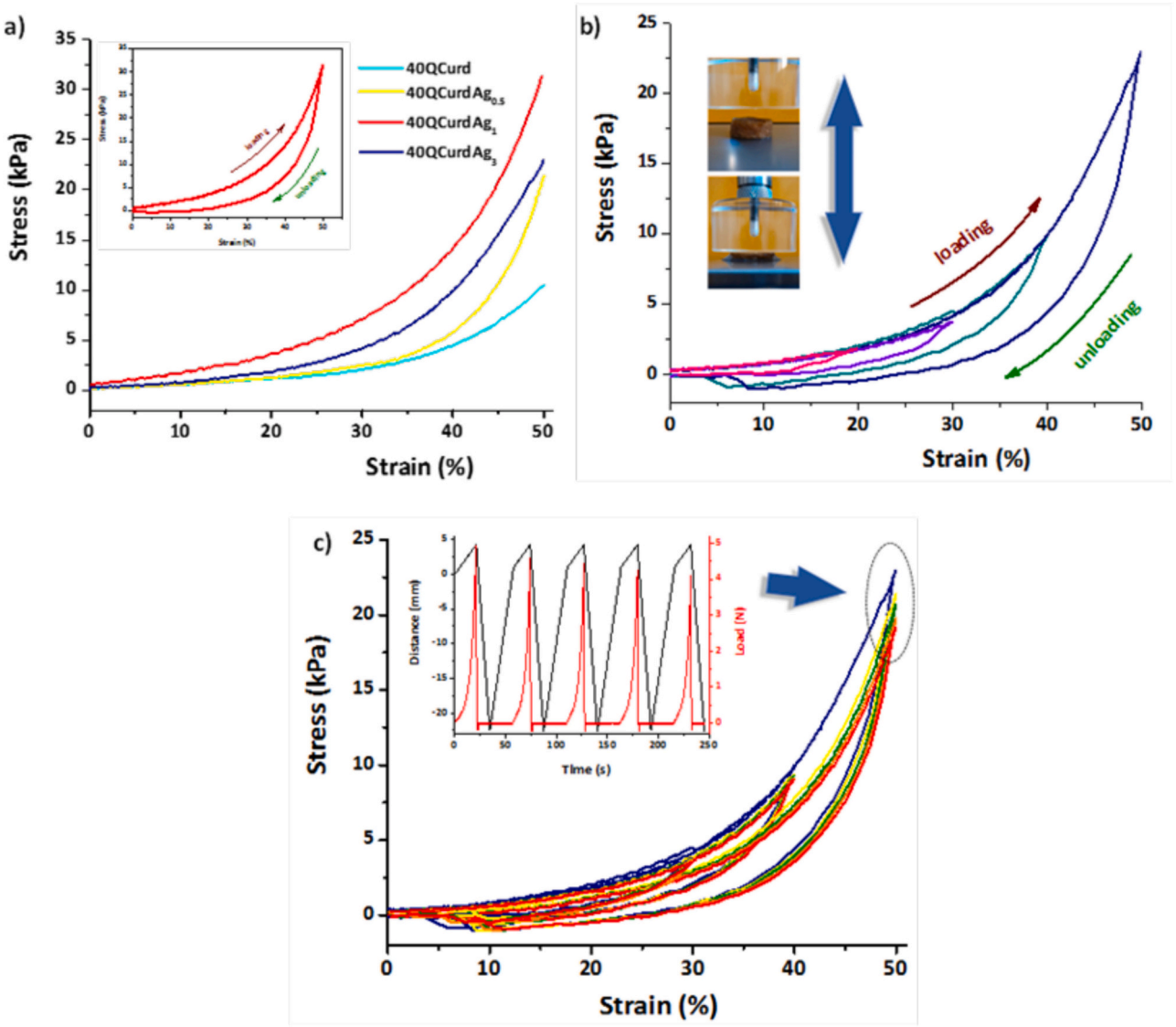

Fig. 6. Mechanical properties: stress–strain curves for 40QCurd-based hydrogels without and with AgNPs-*C.off,* tested in a swollen state (a); loading-unloading curves of 40QCurdAg$_3$ hydrogel at different strain (20%, 30%, 40%, and 50%) (b); hysteresis curves for five successive uniaxial compressive tests of 40QCurdAg$_3$ hydrogel at 50% compression (c).

Table 2
Main mechanical characteristics of 40QCurd-based hydrogels without and with AgNPs-*C.off*.

Sample	Young's modulus* (*E*)	Strength force at 50% compression (σ_{50})	Energy dissipation (50%comp)
	kPa	kPa	kJ/m^3
40QCurd	4.85 ± 0.10	10.52 ± 0.41	0.873 ± 0.08
40QCurdAg$_{0.5}$	10.54 ± 0.51	21.44 ± 0.50	1.012 ± 0.11
40QCurdAg$_1$	11.31 ± 0.38	31.36 ± 0.63	1.916 ± 0.25
40QCurdAg$_3$	6.67 ± 0.20	22.95 ± 0.34	1.510 ± 0.12

* Young's modulus calculated from the slope between 2 and 10% of the linear part of stress-strain curves.

reveal that the hydrogel can recover to its initial state after compression through energy dissipation (Ma et al., 2017; Suflet, Constantin, et al., 2024). In the case of the QCurdAg$_3$ hydrogel (Fig. 6c), at 50% compressive strain over five consecutive cycles, the loading-unloading curves no longer overlapped perfectly, with the maximum load force gradually decreasing as the number of cycles increased (Fig. 6c insert). This behaviour can be attributed to: a) the PBS content that was excluded from the hydrogel after the first compression, which cannot quickly rehydrate the entire structure before the second compression cycle, resulting in lower energy dissipation in the following cycles; b) the rigidity of the structure due to the presence of AgNPs-*C.off*. Such behaviour was not as pronounced in the case of 40QCurd hydrogel (without silver nanoparticles), which exhibited a complete recovery and a good overlap of the five hysteresis loops (Fig. S2). Furthermore, the hysteresis curves of all hydrogels recorded forces below zero (negative values), indicating an adhesion to the stainless-steel surface of the testing device. This behaviour can be attributed to the soft and elastic structure of the hydrogels, as a result of the close relationship between mechanical and adhesive properties. In addition, the presence of the hydrophobic component in the pore structure may also contribute to the enhancement of adhesive properties (Arunbabu et al., 2013; Shan et al., 2022).

3.2.6. *Antioxidant activity*

It is well known that the *C. officinalis* extract possesses significant free radical scavenging activity mainly due to its content of terpenoids, flavonoids, polyphenols, carotenoids, and amino acids (Pelin et al.,

2023; Sapkota & Kunwar, 2024). Some of these phytocompounds play a dual role, contributing to the reduction of Ag^{+} to Ag^{0}, and at the same time, could support wound healing by modulating reactive oxygen species levels and oxidative stress. The antioxidant activity of bio-synthesized AgNPs using plant extracts has also been previously reported (Bedlovicova et al., 2020; Zhangabay & Berillo, 2023). Considering that *C. officinalis* extract contains both water- and alcohol-soluble compounds, the antioxidant activity of AgNPs-*C.off*-loaded QCurd/Curd hydrogels was investigated using two complementary assays: (i) in alcohol medium with the 2,2-diphenyl-1-picrylhydrazyl ($DPPH^{\bullet}$) free radicals, and (ii) in aqueous medium with the 2,2′-azino-bis-(3-ethyl)benzothiazoline-6-sulfonic acid cation radicals ($ABTS^{\bullet+}$). The IC_{50} value of *C. officinalis* hydroalcoholic extract used in this work was determined as 122.67 μg/mL for $DPPH^{\bullet}$ inhibition and 7.12 μg/mL for $ABTS^{\bullet+}$ scavenging (Fig. S3a). The values are consistent with the literature (Preethi et al., 2026).

i) The $DPPH^{\bullet}$ free-radical scavenging activity was also evaluated for both silver nanoparticles and hydrogel samples (Fig. 7a, b). The AgNPs-*C.off* exhibited gradual inhibition, from 1% after 2 h to 41% after 24 h. The DPPH radicals were inhibited much faster in the case of the AgNPs-*C.off* loaded-QCurd/Curd hydrogels, even if the calculated *C. officinalis* extract amount corresponding to the embedded AgNPs-*C.off* is under its IC_{50} value. Thus, the scavenging of $DPPH^{\bullet}$ increase from 18.62% to 2 h to 78.26% after 24 h for $40QCurdAg_{0.5}$. Increasing the content of silver nanoparticles in the hydrogel led to an increase in the DPPH radical scavenging rate. Thus, the 40QCurd Ag_1 and $40QCurdAg_3$ samples achieved a quenching of 95.99% and 97.21%, respectively, after 24 h. In addition, it was observed that the 40QCurd hydrogel (without AgNPs-*C. off*) can scavenge $DPPH^{\bullet}$ from 13.5% (2 h) to 73.2% (24 h) (Fig. S3b). This behaviour can be attributed both to the positive charges of quaternary curdlan derivative (QCurd) (Anraku et al., 2018; Cui et al., 2025) and to the adsorption of $DPPH^{\bullet}$ radicals and their stabilisation through hydrophobic interactions within the hydrogel structure, evidenced by the optical images of hydrogels at the end of the experiment (Fig. S3b). As was expected, the 0QCurd hydrogel (without ionic charges) displayed no $DPPH^{\bullet}$ scavenging activity (Fig. S3b), consistent with the fact that in an alcoholic environment, the hydrogel structure is in a collapsed form, preventing radical adsorption. Overall, the antioxidant activity of $40QCurdAg_x$ hydrogels can be ascribed to a synergistic effect of silver nanoparticles, *C. officinalis* extract, and the cationic charges from curdlan derivative, making these materials promising candidates for biomedical applications where oxidative stress regulation is crucial.

ii) As shown in Fig. 7c, d, the $ABTS^{\bullet+}$ scavenging activity of the 40QCurd hydrogel gradually increased with increasing the AgNPs-*C. off* content during the first 2 h of direct contact with the samples, rising from 13.89% (40QCurd) to 25.33% ($40QCurdAg_3$). After 24 h, the scavenging of $ABTS^{\bullet+}$ was about 100% for all samples. In contrast, the AgNPs-*C.off* nanoparticles alone scavenged 84.5% of $ABTS^{\bullet+}$ radicals within 2 h and maintained this high activity during 24 h. This high scavenging activity is due to the high *C. officinalis* extract content in the corresponding AgNPs-*C.off* used for the experiment (84 fold higher than IC_{50}), its phytocomponents being (Scheme 1), soluble in hydroalcoholic solutions (in this case ethanol: water 1:1), so they can easily contribute to the reduction of $ABTS^{\bullet+}$. In addition, the progressive scavenging of $ABTS^{\bullet+}$ by the 40QCurd hydrogel (sample without AgNPs) can be attributed to both the positive charges of the quaternary ammonium groups from QCurd derivative (Anraku et al., 2018; Cui et al., 2025) and their adsorption into the hydrogel structure by hydrophobic/hydrophilic interactions. This assumption was supported by the scavenging of $ABTS^{\bullet+}$ radicals by the hydrogel without quaternary derivative of curdlan (0QCurd) (Fig. S3c), when the radicals could be retained in the hydrogel structure through hydrophilic interactions and hydrogen bonds.

3.3. Antibacterial assay

The antibacterial activity of *C. officinalis* has been widely reported and is attributed to the presence of oleanolic acid, alkaloids, glycosides, flavonoids, and terpenoids (Muley et al., 2009; Sapkota & Kunwar, 2024). The minimum inhibitory concentration (MIC) of *C. officinalis*

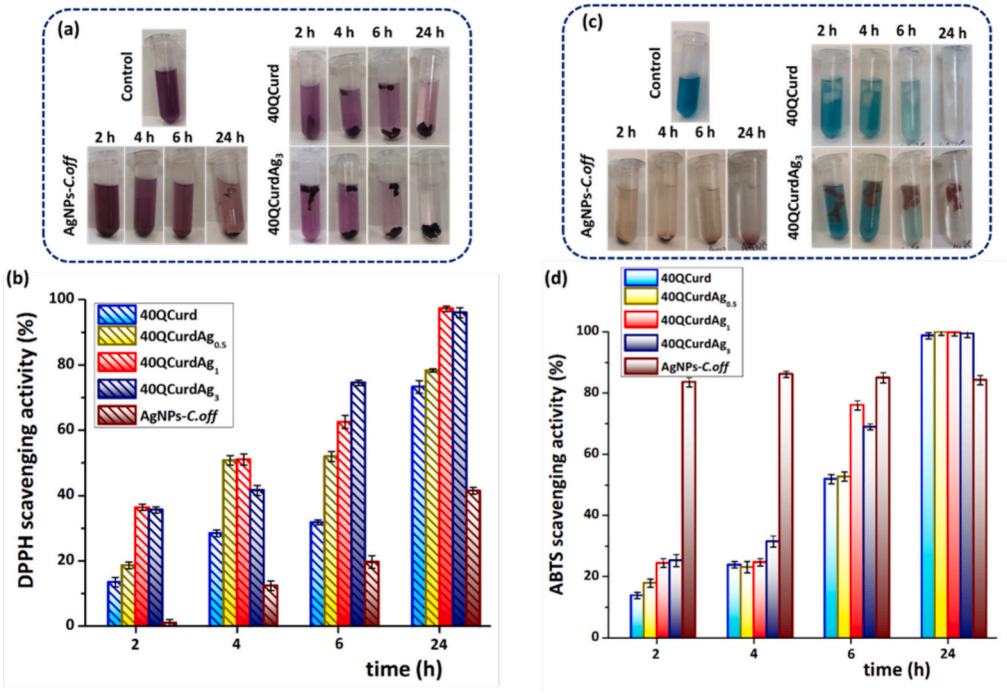

Fig. 7. Antioxidant properties of AgNPs-*C.off* and 40QCurd hydrogels without and with AgNPs-*C.off*: optical images (a) and quantitative $DPPH^{\bullet}$ (b) scavenging activity; optical images of $ABTS^{\bullet+}$ (c) and quantitative $ABTS^{\bullet+}$ (d) scavenging activity.

extracts varies depending on the extraction method, the geographical origin of the plant and the type of extract (e.g. alcoholic or hydro-alcoholic extract, from leaf, flower or root), and the targeted microorganism, with reported values ranging from 6 μg/mL to 100 mg/mL (Abudunia et al., 2017; Pelin et al., 2023; Ruiz-Posadas et al., 2023). Silver nanoparticles (AgNPs) are well established as potent antimicrobial agents effective against Gram-negative and Gram-positive bacteria, including multidrug-resistant strains. Their action is associated with multiple and simultaneous mechanisms of action, and when combined with bioactive compounds from plant extracts or polymeric materials, they can develop a synergistic antimicrobial effect against pathogens such as *S. aureus* and *E. coli* (Bruna et al., 2021).

In this study, the antibacterial effect of the *C. officinalis* extract and AgNPs-*C.off* was evaluated against clinically relevant skin pathogens. The MIC values were determined, showing that the extract alone exhibited a MIC of 5 mg/mL for *S. aureus* (Fig. 8a). In contrast, the AgNPs-*C.off* exhibited significantly higher antibacterial potency with MIC values of 50 μg/mL for *S. aureus* and 25 μg/mL for *E. coli* (Fig. 8b). These MIC values are in agreement with studies reported for AgNPs green-synthesised in the presence of extracts (Dua et al., 2023).

Antimicrobial studies performed on hydrogel materials loaded with drugs or plant extracts have demonstrated increased efficacy using the suspension testing method compared to the disk diffusion test method, due to the sensitivity of the former (Pelin et al., 2023; Suflet, et al., 2024; Suflet, Popescu, et al., 2024). Therefore, the antimicrobial activity of the QCurd-based hydrogels without and with AgNPs-*C.off* was investigated by the *time-kill* method. The antimicrobial effect was evaluated by measuring the vial bacterial counts (Log_{10} CFU/mL) after incubation of bacterial strains (1.5×10^8 CFU/mL) in the presence of hydrogels for 6, 24, 48, and 72 h. As shown in Fig. 8c-d, all hydrogels exhibited a strong antimicrobial effect against *S. aureus* and *E. coli,* which was detectable as early as 6 h of contact. The antimicrobial activity increased over time, leading to complete inhibition (no detected colonies) after 72 h. This effect can be attributed to the quaternary derivative of curdlan, whose intrinsic antimicrobial activity has been previously reported (Popescu et al., 2019; Suflet, Popescu, et al., 2024). As expected, the bacteriostatic and bactericidal effects were significantly enhanced in the hydrogels loaded with AgNPs-*C.off*, with complete inhibition of *S. aureus* growth observed after only 24 h for samples 40QCurdAg$_1$ and 40QCurdAg$_3$ (Fig. 8c), confirming the synergistic effect of the components. For *E. coli* (Fig. 8d), bacterial inhibition followed a similar trend, but with a slightly delayed response compared to *S. aureus*, likely due to differences in cell wall accessibility (Rapacka-Zdonczyk et al., 2021).

3.4. Biocompatibility

Since the newly developed QCurd-based hydrogels are designed for direct contact with human skin, it is essential to ensure that they do not induce adverse effects or cytotoxic responses. Therefore, biocompatibility testing was performed as a crucial step in the development of these materials for potential medical applications. The in vitro assays were carried out using normal human dermal fibroblasts (HDFa, Gibco Invitrogen Cell Culture).

3.4.1. MTT assay and cell morphology

The antimicrobial activity of AgNPs, attributed to the oxidative activity and the release of silver ions into the biological environment, induces a series of negative effects on cellular structure and functions, ultimately leading to cytotoxicity, genotoxicity, immunological responses and cell death (Akter et al., 2018). Recent studies have reported that the green synthesis of AgNPs allows obtaining metal NPs with reduced biological and cytological compatibility (Sati et al., 2025). In our studies, the MTT assay results showed that none of the tested hydrogels reduced cell viability below the critical threshold of 80% throughout the entire experimental period (Fig. 9a). At 24 h and 48 h, both the control hydrogel without nanoparticles (40QCurd) and those containing low concentrations of AgNPs-*C.off* (40QCurdAg$_{0.5}$ and 40QCurdAg$_1$) maintain a cell viability above 93%. In contrast, the 40QCurdAg$_3$ hydrogels (with the highest nanoparticles content) exhibited a moderate reduction in viability, decreasing to 91% at 24 h and 81% at 48 h. After 72 h of exposure, no significant differences were recorded between samples, with cell viability values ranging between

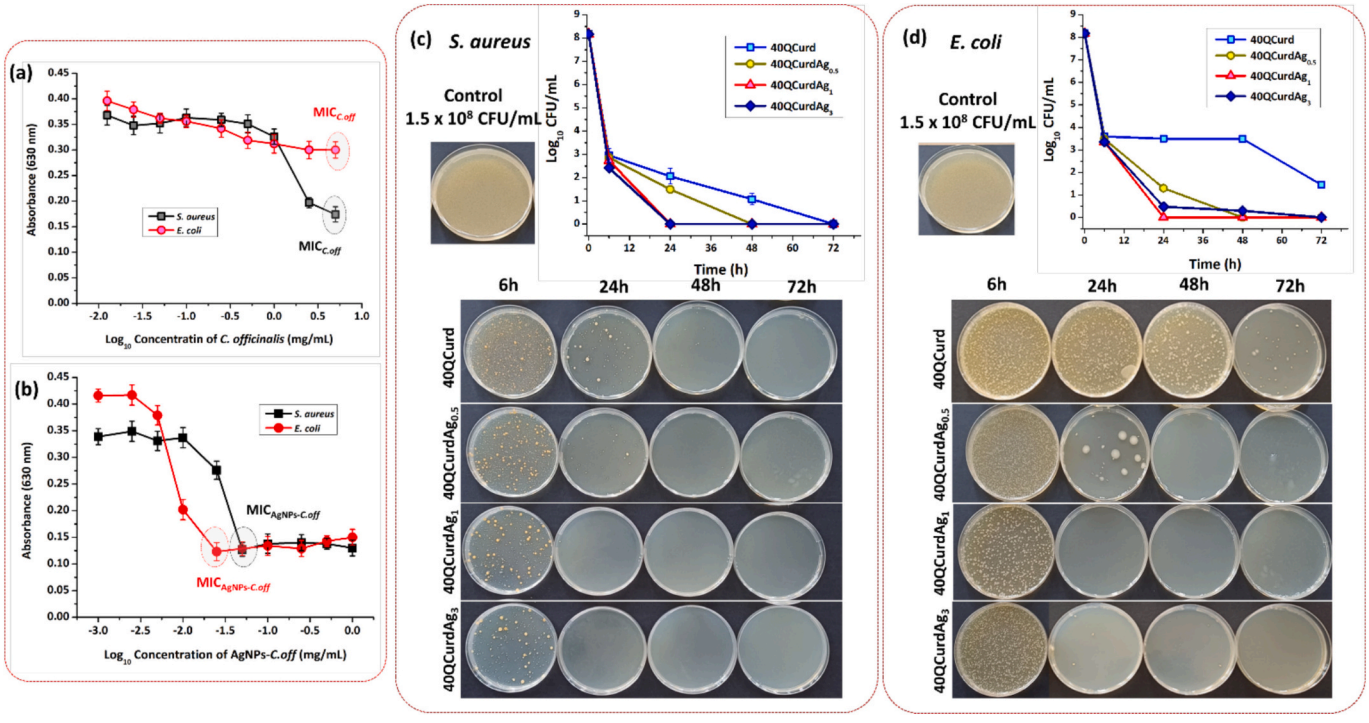

Fig. 8. The minimum inhibitory concentration against *S. aureus* and *E. coli*: *C. officinalis* extract (a); silver nanoparticles bio-synthesised in the presence of *C. officinalis* extract (b). Antibacterial activity of QCurd-based hydrogels loaded with AgNPs-*C.off* against *S. aureus* (c) and *E. coli* (d).

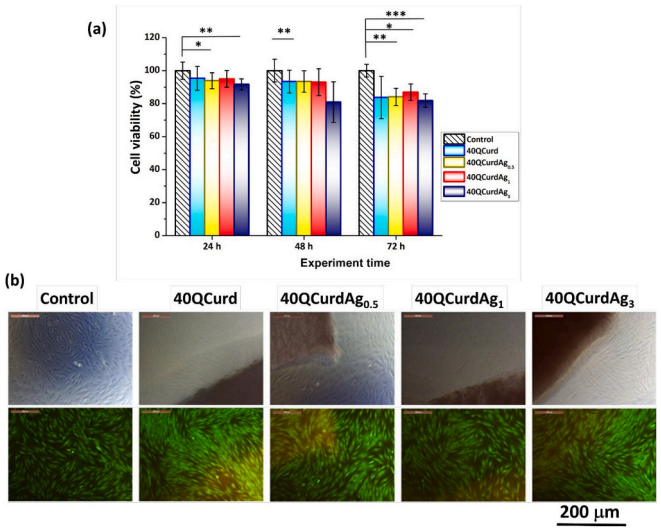

Fig. 9. Cell viability data from the MTT assays (a) and microscopic images of HDFa cells morphology (b) for QCurd-based hydrogels without and with AgNPs-*C.off*. Results are expressed as means ± standard deviations (S.D.) of three experiments. *$p < 0.05$, **$p < 0.01$, ***$p < 0.001$ vs control.

82% and 87%. According to the ISO 10993-5 (ISO 10993-5, 2009) standard for the biological evaluation of medical devices, a material is considered non-cytotoxic if cell viability remains above 70%. Based on this criterion, all hydrogels, regardless of AgNPs-*C.off* content, can be classified as non-cytotoxic. Overall, the MTT assay confirms that QCurd-based hydrogels do not release cytotoxic compounds, suggesting their suitability for further biomedical applications.

Fig. 9b show the representative images of fibroblast cells in contact with the QCurd-based hydrogels, both in bright field and fluorescence. The micrographs (Fig. 9b) clearly show that the presence of the hydrogels, either with or without AgNPs-*C.off*, did not affect the density, size or morphology of the cells. Cells exhibited normal HDF-specific growth patterns and behaviour, and maintained a uniform distribution across the culture surface. Moreover, the presence of actively dividing cells was observed, and no morphological indicators of apoptosis or cytotoxic stress were detected. This finding further supports the good biocompatibility of samples.

3.4.2. *Wound healing assay*

Cell migration plays a crucial role in wound healing, as the inflammatory phase promotes fibroblast migration and proliferation, which are essential for the synthesis of the new extracellular matrix (Talbott et al., 2022). The wound healing assay offers information on the migration of the cells into an artificially created gap, under the influence of the tested materials. Regarding this aspect, this scratch assay was performed to evaluate the influence of QCurd/Curd-based hydrogels on fibroblast migration. As shown in Fig. 10, fibroblasts display progressive migration into the scratched area over time. Quantitative analysis of cell migration at 8 h, compared to time 0, revealed a pronounced migration in the case of the 40QCurdAg$_1$ sample (Fig. 10b).

After 24 h, the scratched area was completely covered with cells for all tested hydrogels (Fig. 10a), demonstrating efficient cell migration. Moreover, compared to the control sample, the hydrogel-treated samples exhibited a higher density of migrated cells, indicating that the QCurd/Curd-based hydrogels promote fibroblast mobility and exert a positive effect on the wound healing process.

4. Conclusions

Novel cationic curdlan-based hydrogels containing green-synthesised silver nanoparticles decorated with *Calendula officinalis* phytocomponents were successfully developed through the covalent cross-linking of quaternized curdlan and native curdlan.

The synthesis parameters of AgNPs-*C.off* were optimized, and nanoparticle formation was confirmed by UV–Vis spectroscopy, TEM, XRD, and FT-IR analyses. The obtained silver nanoparticles exhibited a face-centred cubic crystalline structure and an average diameter of 22 ± 0.19 nm.

The resulting hydrogels displayed a homogeneous porous architecture with interconnected pores, appropriate swelling behaviour under

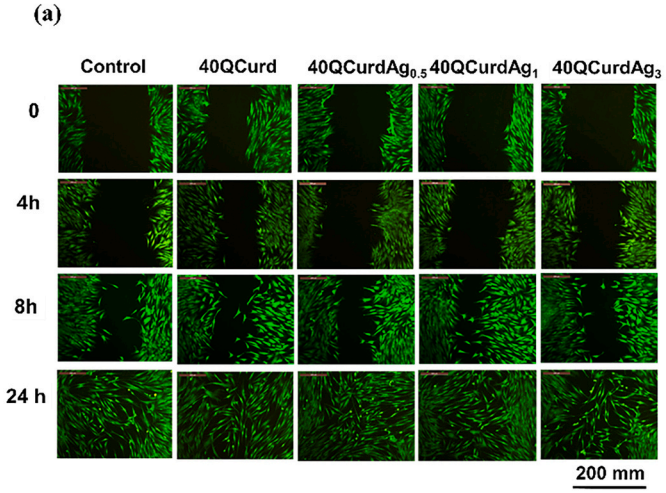

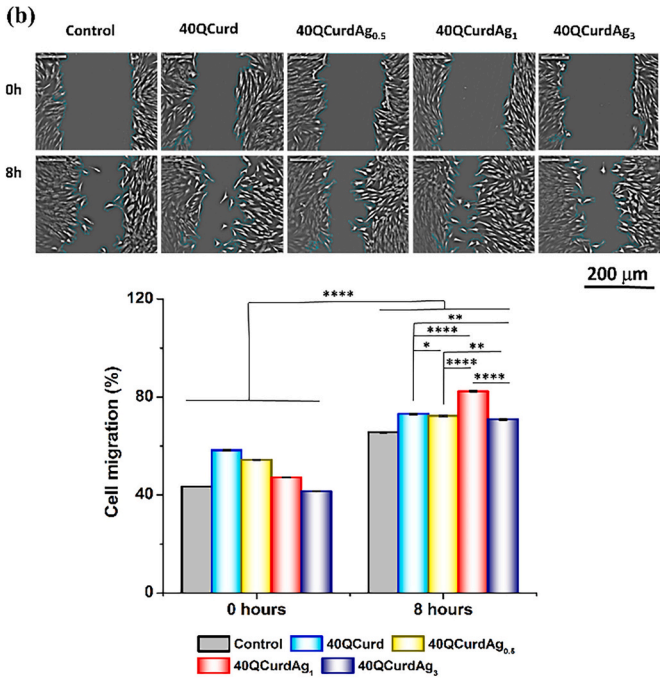

Fig. 10. Cell migration from the initial scratch to 24 h (a). Quantitative analysis of the cell migration at 8 h compared to moment 0 – the percent area covered by the cells (b). Results are expressed as means ± standard deviations (S.D.) of three experiments. *p < 0.05, **p < 0.01, ****$p < 0.0001$ vs control.

simulated skin conditions, and excellent elastic recovery after five consecutive compression cycles.

Biological evaluation demonstrated that all hydrogels were cytocompatible towards human dermal fibroblasts and promoted cell migration in the wound-healing assay. Furthermore, the materials exhibited antioxidant activity and antibacterial effects against both *S. aureus* and *E. coli*, which were further enhanced by the incorporation of AgNPs-*C.off*. These findings indicate that the synergistic combination of cationic curdlan, silver nanoparticles, and *C. officinalis* phytocomponents constitutes a promising strategy for the development of multifunctional wound-dressing materials.

The developed hydrogels offer several advantages, including the use of renewable polysaccharides, a green route for nanoparticle synthesis, the intrinsic antibacterial activity of the cationic curdlan derivative, and the combined antioxidant and antimicrobial properties imparted by the incorporated AgNPs-*C.off*.

Future studies will focus on enhancing the biological performance of the developed hydrogels and conducting in vivo investigations to assess their potential for clinical translation as advanced wound-dressing materials.

CRediT authorship contribution statement

Dana M. Suflet: Writing – review & editing, Writing – original draft, Validation, Project administration, Methodology, Investigation, Funding acquisition, Conceptualization. **Irina Popescu:** Writing – original draft, Visualization, Methodology. **Andreea Luca:** Writing – original draft, Methodology, Formal analysis. **Maria Butnaru:** Writing – original draft, Visualization, Methodology. **Cristina M. Rîmbu:** Writing – original draft, Visualization, Methodology, Formal analysis. **Cristina E. Horhogea:** Writing – original draft, Formal analysis. **Marieta Constantin:** Writing – review & editing, Validation, Supervision, Methodology, Conceptualization.

Declaration of competing interest

The authors declare that they have no known competing financial interests or personal relationships that could have appeared to influence the work reported in this paper.

Acknowledgments

This work was supported by a grant of the Romanian Ministry of Research, Innovation and Digitalization, CCCDI - UEFISCDI, project number PN-IV-P7-7.1-PED-2024-1639, within PNCDI IV.

Appendix A. Supplementary data

Supplementary data to this article can be found online at https://doi.org/10.1016/j.carbpol.2026.125623.

Data availability

No data was used for the research described in the article.

References

Abudunia, A.-M., Marmouzi, I., Faouzi, M. E. A., Ramli, Y., Taoufik, J., El Madani, N., Essassi, E. M., Salama, A., Khedid, K., Ansar, M., & Ibrahimi, A. (2017). Anticandidal, antibacterial, cytotoxic and antioxidant activities of *Calendula arvensis* flowers. *Journal de Mycologie Médicale, 27*(1), 90–97. https://doi.org/10.1016/j.mycmed.2016.11.002

Akter, M., Sikder, M. T., Rahman, M. M., Ullah, A. K. M. A., Hossain, K. F. B., Banik, S., … Kurasaki, M. (2018). A systematic review on silver nanoparticles-induced cytotoxicity: Physicochemical properties and perspectives. *Journal of Advanced Research, 9*, 1–16. https://doi.org/10.1016/j.jare.2017.10.008

Anraku, M., Gebicki, J. M., Iohara, D., Tomida, H., Uekama, K., Maruyama, T., Hirayama, F., & Otagiri, M. (2018). Antioxidant activities of chitosan and its derivatives in in vitro and in vivo studies. *Carbohydrate Polymers, 199*, 141–149. https://doi.org/10.1016/j.carbpol.2018.07.016

Ansari, M., Ahmed, S., Abbasi, A., et al. (2023). Plant mediated fabrication of silver nanoparticles, process optimization, and impact on tomato plant. *Scientific Reports, 13*, 18048. https://doi.org/10.1038/s41598-023-45038-x

Arif, R., & Uddin, R. (2021). A review on recent developments in the biosynthesis of silver nanoparticles and its biomedical applications. *Medicinal Devices & Sensors, 4*, 1–20. https://doi.org/10.1002/mds3.10158

Arunachalam, K., & Sreeja, P. S. (2025). MTT assay protocol. In *Advanced cell and molecular techniques. Springer Protocols Handbooks*. New York, NY: Humana. https://doi.org/10.1007/978-1-0716-4518-5_45.

Arunbabu, D., Shahsavan, H., Zhang, W., & Zhao, B. (2013). Poly(AAc-co-MBA) hydrogel films: Adhesive and mechanical properties in aqueous medium. *The Journal of Physical Chemistry B, 117*(1), 441–449. https://doi.org/10.1021/jp3101688

Baghizadeh, A., Ranjbar, S., Gupta, V. K., Asif, M., Pourseyedi, S., Karimi, M. J., & Mohammadinejad, R. (2015). Green synthesis of silver nanoparticles using seed extract of Calendula officinalis in liquid phase. *Journal of Molecular Liquids, 207*, 159–163. https://doi.org/10.1016/j.molliq.2015.03.029

Batain, F., Crescencio, K., Alves, T., Souza, J. F., Amaral, V., Castro, J., Santos, C., Jozala, A., Lopes, L., & Chaud, M. (2020). Medicinal plant extract associated with bacterial cellulose membrane: Antibacterial activity and physicochemical properties. *Archives of Pharmacy and Pharmaceutical Sciences, 4*, 013–020. https://doi.org/10.29328/journal.apps.1001022

Bedlovicova, Z., Strapac, I., Balaz, M., & Salayova, A. (2020). A brief overview on antioxidant activity determination of silver nanoparticles. *Molecules, 25*, Article 3191. https://doi.org/10.3390/molecules25143191

Bruna, T., Maldonado-Bravo, F., Jara, P., & Caro, N. (2021). Silver nanoparticles and their antibacterial applications. *International Journal of Molecular Sciences, 22*, Article 7202. https://doi.org/10.3390/ijms22137202

Castano, O., Perez-Amodio, S., Navarro-Requena, C., Mateos-Timoneda, M. A., & Engel, E. (2018). Instructive microenvironments in skin wound healing: Biomaterials as signal releasing platforms. *Advanced Drug Delivery Reviews, 129*, 95–117. https://doi.org/10.1016/j.addr.2018.03.012

Catauro, M., Barrino, F., Dal Poggetto, G., Crescente, G., Piccolella, S., & Pacifico, S. (2020). New SiO2/caffeic acid hybrid materials: Synthesis, spectroscopic characterization, and bioactivity. *Materials, 13*(2), Article 394. https://doi.org/10.3390/ma13020394

Chaudhari, V., Buttar, H. S., Bagwe-Parab, S., Tuli, H. S., Vora, A., & Kaur, G. (2021). Therapeutic and industrial applications of curdlan with overview on its recent patents. *Frontiers in Nutrition, 8*, Article 646988. https://doi.org/10.3389/fnut.2021.646988

Chen, M., & Liang, P. (2017). Synthesis and antibacterial activity of quaternized curdlan. *Polymer Bulletin, 74*, 4251–4266. https://doi.org/10.1007/s00289-017-1951-0

Chen, Y., & Wang, F. (2020). Review on the preparation, biological activities and applications of curdlan and its derivatives. *European Polymer Journal, 141*, Article 110096. https://doi.org/10.1016/j.eurpolymj.2020.110096

Chugh, D., Viswamalya, V. S., & Das, B. (2021). Green synthesis of silver nanoparticles with algae and the importance of capping agents in the process. *Journal of Genetic Engineering and Biotechnology, 19*, 126. https://doi.org/10.1186/s43141-021-00228-w

CLSI (Ed.). (2010). *Methods for antimicrobial dilution and disk susceptibility of infrequently isolated or fastidious Bacteria, approved guideline, 2nd ed.; CLSI document M45-A2*. Wayne, PA, USA: clinical and laboratory standards institute. https://clsi.org/shop/standards/m45.

CLSI (Ed.). (2012). *Methods for dilution antimicrobial susceptibility tests for Bacteria that grow aerobically, approved standard, 9th ed.; CLSI document M07-A9*. Wayne, PA, USA: clinical and laboratory standards institute. https://clsi.org/shop/standards/m07.

Coates, J., & John, E. (2000). Interpretation of infrared spectra: A practical approach. In R. A. Meyers (Ed.), *Encyclopedia of analytical chemistry* (pp. 10815–10837). Chichester, UK: Wiley & Sons Ltd.

Constantin, M., Spiridon, M., Ichim, D. L., Daraba, O. M., Suflet, D. M., Ignat, M., & Fundueanu, G. (2023). Synthesis, biological and catalytic activity of silver nanoparticles generated and covered by oxidized pullulan. *Materials Chemistry and Physics, 295*, Article 127141. https://doi.org/10.1016/j.matchemphys.2022.127141

Cui, J., Sun, Y., Wang, L., Ji, Y., Zhao, H., Sun, M., Guo, Z., & Dong, F. (2025). Quaternary ammonium salts of chitosan containing aromatic ring: Synthesis, characterization, antimicrobial, antioxidant and cytotoxicity. *Carbohydrate Research, 552*, Article 109431. https://doi.org/10.1016/j.carres.2025.109431

Dhaka, A., Mali, S. C., Sharma, S., & Trivedi, R. (2023). A review on biological synthesis of silver nanoparticles and their potential applications. *Results in Chemistry, 6*, Article 101108. https://doi.org/10.1016/j.rechem.2023.101108

Ding, L., Song, S., Chen, L., Shi, J., Zhao, B., Teng, G., & Zhang, J. (2021). A freeze-thawing method applied to the fabrication of 3-d curdlan/polyvinyl alcohol hydrogels as scaffolds for cell culture. *International Journal of Biological Macromolecules, 174*, 101–109. https://doi.org/10.1016/j.ijbiomac.2021.01.160

Ding, Q., Mo, Z., Wang, X., Chen, M., Zhou, F., Liu, Z., Long, Y., Xia, X., & Zhao, P. (2024). The antibacterial and hemostatic curdlan hydrogel–loading epigallocatechin gallate for facilitating the infected wound healing. *International Journal of Biological Macromolecules, 266*(Part 1), Article 131257. https://doi.org/10.1016/j.ijbiomac.2024.131257

Downer, M., Berry, C. E., Parker, J. B., Kameni, L., & Griffin, M. (2023). Current biomaterials for wound healing. *Bioengineering (Basel), 10*(12), Article 1378. https://doi.org/10.3390/bioengineering10121378

Dua, T. K., Giri, S., Nandi, G., Sahu, R., Shaw, T. K., & Paul, P. (2023). Green synthesis of silver nanoparticles using Eupatorium adenophorum leaf extract: Characterizations,

antioxidant, antibacterial and photocatalytic activities. *Chemical Papers, 77*, 2947–2956. https://doi.org/10.1007/s11696-023-02676-9

Feng, W., & Wang, Z. (2023). Tailoring the swelling-shrinkable behavior of hydrogels for biomedical applications. *Advanced Science, 10*(28), Article 2303326. https://doi.org/10.1002/advs.202303326

Gilbert, D. F., & Boutros, M. (2016). A protocol for a high-throughput multiplex cell viability assay. In D. Azorsa, & S. Arora (Eds.), *1470. High-throughput RNAi screening. Methods in molecular biology*. New York, NY: Humana Press. https://doi.org/10.1007/978-1-4939-6337-9_6.

Hatano, I., Mochizuki, K., Sumi, T., & Koga, K. (2016). Hydrophobic polymer chain in water that undergoes a coil-to-globule transition near room temperature. *Journal of Physical Chemistry B, 120*, 12127–12134. https://doi.org/10.1021/acs.jpcb.6b08347

He, Y., Wei, F., Ma, Z., Zhang, H., Yang, Q., Yao, B., … Zhang, Q. (2017). Green synthesis of silver nanoparticles using seed extract of *Alpinia katsumadai*, and their antioxidant, cytotoxicity, and antibacterial activities. *RSC Advances, 7*, Article 39842. https://doi.org/10.1039/C7RA05286C

Hemlata, H., Meena, P. R., Singh, A. P., & Tejavath, K. K. (2020). Biosynthesis of silver nanoparticles using *Cucumis prophetarum* aqueous leaf extract and their antibacterial and antiproliferative activity against cancer cell lines. *ACS Omega, 5*(10), 5520–5528. https://doi.org/10.1021/acsomega.0c00155

Iravani, S., Korbekandi, H., Mirmohammadi, S. V., & Zolfaghari, B. (2014). Synthesis of silver nanoparticles: Chemical, physical and biological methods. *Research in Pharmaceutical Sciences, 9*(6), 385–406. https://pubmed.ncbi.nlm.nih.gov/26339255/.

ISO 10993-5. (2009). *Biological evaluation of medical devices. Part 5: Tests for in vitro cytotoxicity*. https://www.iso.org/standard/36406.html.

Jagtap, U. B., & Bapat, V. A. (2013). Green synthesis of silver nanoparticles using *Artocarpus heterophyllus lam.* Seed extract and its antibacterial activity. *Industrial Crops and Products, 46*, 132–137. https://doi.org/10.1016/j.indcrop.2013.01.019

Jonkman, J. E. N., Cathcart, J. A., Xu, F., Bartolini, M. E., Amon, J. E., Stevens, K. M., & Colarusso, P. (2014). An introduction to the wound healing assay using live-cell microscopy. *Cell Adhesion & Migration, 8*(5), 440–451. https://doi.org/10.4161/cam.36224

Joshi, S., Maan, M., Barman, P., Sharely, I., Verma, K., Preet, S., & Saini, A. (2025). Advances in biomaterials for wound care management: Insights from recent developments. *Advances in Colloid and Interface Science, 343*, Article 103563. https://doi.org/10.1016/j.cis.2025.103563

Kozlowska, J., Stachowiak, N., & Sionkowska, A. (2018). Collagen/gelatin/hydroxyethyl cellulose composites containing microspheres based on collagen and gelatin: Design and evaluation. *Polymers, 10*, Article 456. https://doi.org/10.3390/polym10040456

Lambert, R. J. W., & Pearson, J. (2000). Susceptibility testing: Accurate and reproducible minimum inhibitory concentration (MIC) and non-inhibitory concentration (NIC) values. *Journal of Applied Microbiology, 88*, 784–790. https://doi.org/10.1046/j.1365-2672.2000.01017.x

Lan, X., Du, T., Zhuo, J., Wang, T., Shu, R., Li, Y., Zhang, W., Ji, Y., Wang, Y., Yue, X., & Wang, J. (2024). Advances of biomacromolecule-based antibacterial hydrogels and their performance evaluation for wound healing: A review. *International Journal of Biological Macromolecules, 279*, Article 135577. https://doi.org/10.1016/j.ijbiomac.2024.135577

Le Bourvellec, C., & Renard, C. M. G. C. (2012). Interactions between polyphenols and macromolecules: Quantification methods and mechanisms. *Critical Reviews in Food Science and Nutrition, 52*(3), 213–248. https://doi.org/10.1080/10408398.2010.499808

Li, Y., Han, Y., Li, H., Niu, X., Zhang, D., & Wang, K. (2024). Antimicrobial hydrogels: Potential materials for medical application. *Small, 20*, Article 2304047. https://doi.org/10.1002/smll.202304047

Liang, L., Su, Q., Ma, Y., Zhao, S., Zhang, H., & Gao, X. (2024). Research progress on the polysaccharide extraction and antibacterial activity. *Annals of Microbiology, 74*, Article 17. https://doi.org/10.1186/s13213-024-01762-x

Liu, X., Chen, J.-L., Yang, W.-Y., Qian, Y.-C., Pan, J.-Y., Zhu, C.-N., Liu, L., Ou, W.-B., Zhao, H.-X., & Zhang, D.-P. (2021). Biosynthesis of silver nanoparticles with antimicrobial and anticancer properties using two novel yeasts. *Scientific Reports, 11*, 15795 (2021) https://doi.org/10.1038/s41598-021-95262-6.

Ma, X. M., Li, R., Ren, J., Lv, X. C., Zhao, X. H., Ji, Q., & Xi, Y. Z. (2017). Restorable, high-strength poly(Nisopropylacrylamide) hydrogels constructed through chitosan-based dual macro-cross-linkers with rapid response to temperature jumps. *RSC Advances, 7*, 47767–47774. https://doi.org/10.1039/C7RA10148A

Majtan, J., & Jesenak, M. (2018). B-Glucans: Multi-functional modulator of wound healing. *Molecules, 23*, Article 806. https://doi.org/10.3390/molecules23040806

Meenalotchani, R., Nirenjen, S., Manisha, M., Prajapati, B. G., Arun, E., Afreen, N., … Alsaidan, O. A. (2025). Recent advances in silver nanoparticles for enhanced wound healing with mechanisms, formulations, and clinical insights. *Journal of Drug Delivery Science and Technology, 114*(A), Article 107437. https://doi.org/10.1016/j.jddst.2025.107437

Minsart, M., Vlierberghe, S. V., Dubruel, P., & Mignon, A. (2022). Commercial wound dressings for the treatment of exuding wounds: An in-depth physico-chemical comparative study. *Burns & Trauma, 10*, Article tkac024. https://doi.org/10.1093/burnst/tkac024

Mittal, A. K., Chisti, Y., & Banerjee, U. C. (2013). Synthesis of metallic nanoparticles using plant extracts. *Biotechnology Advances, 31*, 346–356. https://doi.org/10.1016/j.biotechadv.2013.01.003

Mukhtar, H., Ansari, S. H., Ali, M., & Naved, T. (2004). A new d-lactone containing triterpene from the flowers of *Calendula officinalis*. *Pharmaceutical Biology, 42*(4–5), 305–307. https://doi.org/10.1080/13880200490511873

Muley, B. P., Khadabadi, S. S., & Banarase, N. B. (2009). Phytochemical constituents and pharmacological activities of *Calendula officinalis* Linn (Asteraceae): A review. *Tropical Journal of Pharmaceutical Research, 8*, 455–465. https://doi.org/10.4314/tjpr.v8i5.48090

Naseri-Nosar, M., & Ziora, Z. M. (2018). Wound dressings from naturally-occurring polymers: A review on homopolysaccharide-based composites. *Carbohydrate Polymers, 189*, 379–398. https://doi.org/10.1016/j.carbpol.2018.02.003

Nasra, S., Patel, M., Shukla, H., Bhatt, M., & Kumar, A. (2023). Functional hydrogel-based wound dressings: A review on biocompatibility and therapeutic efficacy. *Life Sciences, 334*, Article 122232. https://doi.org/10.1016/j.lfs.2023.122232

Nenitescu, C. D. (1966). *Organic chemistry* (4th ed.) (4th ed.,. *1*. Bucharest: Didactic and Pedagogical Publishing House.

Niculescu, A.-G., & Grumezescu, A. M. (2022). An up-to-date review of biomaterials application in wound management. *Polymers, 14*, Article 421. https://doi.org/10.3390/polym14030421

Oselusi, S. O., Sibuyi, N. R. S., Meyer, M., & Madiehe, A. M. (2024). Phytonanotherapeutic applications of plant extract-synthesized silver nanoparticles in wound healing — A prospective overview. *BioNanoScience, 14*, 3455–3475. https://doi.org/10.1007/s12668-024-01535-5

Ounkaew, A., Jarensungnen, C., Jaroenthai, N., et al. (2023). Fabrication of hydrogel-nano silver based on *Aloe vera*/carboxymethyl cellulose/tannic acid for antibacterial and pH-responsive applications. *Journal of Polymers and the Environment, 31*, 50–63. https://doi.org/10.1007/s10924-022-02611-1

Ounkaew, A., Kasemsiri, P., Jetsrisuparb, K., Uyama, H., Hsu, Y.-I., Boonmars, T., … Chindaprasirt, P. (2020). Synthesis of nanocomposite hydrogel based carboxymethyl starch/polyvinyl alcohol/nanosilver for biomedical materials. *Carbohydrate Polymers, 248*, Article 116767. https://doi.org/10.1016/j.carbpol.2020.116767

Parikh, D., Fink, T., DeLucca, A., & Parikh, A. (2011). Absorption and swelling characteristics of silver (I) antimicrobial wound dressings. *Textile Research Journal, 81*, 494–503. https://doi.org/10.1177/0040517510380778

Patel, D. K., Jung, E., Priya, S., Won, S.-Y., & Han, S. S. (2024). Recent advances in biopolymer-based hydrogels and their potential biomedical applications. *Carbohydrate Polymers, 323*, Article 121408. https://doi.org/10.1016/j.carbpol.2023.121408

Patel, H., & Joshi, J. (2023). Green and chemical approach for synthesis of Ag_2O nanoparticles and their antimicrobial activity. *Journal of Sol-Gel Science and Technology, 105*, 814–826. https://doi.org/10.1007/s10971-023-06036-7

Pelin, I. M., Silion, M., Popescu, I., Rîmbu, C. M., Fundueanu, G., & Constantin, M. (2023). Pullulan/poly(vinyl alcohol) hydrogels loaded with *Calendula officinalis* extract: Design and in vitro evaluation for wound healing applications. *Pharmaceutics, 15*, Article 1674. https://doi.org/10.3390/pharmaceutics15061674

Popescu, I., Pelin, I. M., Ailiesei, G. L., Ichim, D. L., & Suflet, D. M. (2019). Amphiphilic polysaccharide based on curdlan: Synthesis and behaviour in aqueous solution. *Carbohydrate Polymers, 224*, Article 115157. https://doi.org/10.1016/j.carbpol.2019.115157

Prasad, T. N. V. K. V., Kambala, V. S. R., & Naidu, R. (2013). Phyconanotechnology: Synthesis of silver nanoparticles using brown marine algae *Cystophora moniliformis* and their characterisation. *Journal of Applied Phycology, 25*, 177–182. https://doi.org/10.1007/s10811-012-9851-z

Preethi, K. C., Kuttan, G., & Kuttan, R. (2026). Antioxidant potential of an extract of *Calendula officinalis*. Flowers in vitro and in vivo. *Pharmaceutical Biology, 44*, 691–697. https://doi.org/10.1080/13880200601009149

Rapacka-Zdonczyk, A., Wozniak, A., Michalska, K., Pieranski, M., Ogonowska, P., Grinholc, M., & Nakonieczna, J. (2021). Factors determining the susceptibility of bacteria to antibacterial photodynamic inactivation. *Frontiers in Meddicine, 8*, Article 642609. https://doi.org/10.3389/fmed.2021.642609

Re, R., Pellegrini, N., Proteggente, A., Pannala, A., Yang, M., & Rice-Evans, C. (1999). Antioxidant activity applying an improved ABTS radical cation decolorization assay. *Free Radical Biology and Medicine, 26*, 1231–1237. https://doi.org/10.1016/S0891-5849(98)00315-3

Ruiz-Posadas, L.d. M., Rodriguez-Lopez, V. A., Cadena-Iniguez, J., Delgadillo-Martinez, J., San Miguel-Chavez, R., Salazar-Aguilar, S., & Valdez-Carrasco, J. (2023). Antibacterial activity of the *Calendula officinalis* L. essential oil on *Escherichia coli*. *Agro Productividad, 16*, 25–31. https://doi.org/10.32854/agrop.v15i4.2520

Sabir, S. M., Khan, M. F., Rocha, J. B. T., Boligon, A. A., & Athayde, M. L. (2015). Phenolic profile, antioxidant activities and genotoxic evaluations of *Calendula officinalis*. *Journal of Food Biochemistry, 39*, 316–324. https://doi.org/10.1111/jfbc.12132

Santos, A. P., Gonçalves, M. M., Justus, B., Fardin, D. P. S., Toledo, A. C. O., Budel, J. M., & Paula, J. P. (2022). *Calendula officinalis L. flower extract-mediated green synthesis of silver nanoparticles under LED light. Brazilian Journal of Pharmaceutical Sciences, 58*, Article e19519. https://doi.org/10.1590/s2175-97902022e19519

Sapkota, B., & Kunwar, P. (2024). A review on traditional uses, phytochemistry and pharmacological activities of *Calendula officinalis* Linn. *Natural Product Communications, 19*(6), 1–22. https://doi.org/10.1177/1934578X241259021

Sati, A., Ranade, T. N., Mali, S. N., Yasin, H. K. A., & Pratap, A. (2025). Silver nanoparticles (AgNPs): Comprehensive insights into bio/synthesis, key influencing factors, multifaceted applications, and toxicity – A 2024 update. *ACS Omega, 10*(8), 7549–7582. https://doi.org/10.1021/acsomega.4c11045

Shan, C., Che, M., Cholewinski, A., KI Kunihiro, J., Yim, E. K. F., Su, R., & Zhao, B. (2022). Adhesive hydrogels tailored with cellulose nanofibers and ferric ions for highly sensitive strain sensors. *Chemical Engineering Journal, 450*, Article 138256. https://doi.org/10.1016/j.cej.2022.138256

Sharma, V. K., Yngard, R. A., & Lin, Y. (2009). Silver nanoparticles: Green synthesis and their antimicrobial activities. *Advances in Colloid and Interface Science, 145*(1–2), 83–96. https://doi.org/10.1016/j.cis.2008.09.002

Shrestha, S., Wang, B., & Dutta, P. K. (2024). Commercial silver-based dressings: In vitro and clinical studies in treatment of chronic and burn wounds. *Antibiotics (Basel), 13*, Article 910. https://doi.org/10.3390/antibiotics13090910

Su, J., Li, J., Liang, J., Zhang, K., & Li, J. (2021). Hydrogel preparation methods and biomaterials for wound dressing. *Life (Basel), 11*, Article 1016. https://doi.org/10.3390/life11101016

Suflet, D. M., Constantin, M., Pelin, I. M., Popescu, I., Rimbu, C. M., Horhogea, C. E., & Fundueanu, G. (2024). Chitosan–oxidized pullulan hydrogels loaded with essential clove oil: Synthesis, characterization, antioxidant and antimicrobial properties. *Gels, 10*, Article 227. https://doi.org/10.3390/gels10040227

Suflet, D. M., Popescu, I., Pelin, I. M., Ichim, D. L., Daraba, O. M., Constantin, M., & Fundueanu, G. (2021). Dual cross-linked chitosan/PVA hydrogels containing silver nanoparticles with antimicrobial properties. *Pharmaceutics, 13*, Article 1461. https://doi.org/10.3390/pharmaceutics13091461

Suflet, D. M., Popescu, I., Prisecaru, A. I., & Pelin, I. M. (2021). Synthesis and characterization of curdlan – phosphorylated curdlan based hydrogels for drug release. *International Journal of Polymeric Materials and Polymeric Biomaterials, 70* (12), 1–10. https://doi.org/10.1080/00914037.2020.1765360

Suflet, D. M., Popescu, I., Stanciu, M.-C., & Rimbu, C. M. (2024). Antimicrobial hydrogels based on cationic curdlan derivatives for biomedical applications. *Gels, 10*, Article 424. https://doi.org/10.3390/gels10070424

Tak, U. N., Rashid, S., Kour, P., Nazir, N., Zargar, M. I., & Dar, A. A. (2023). *Bergenia stracheyi* extract-based hybrid hydrogels of biocompatible polymers with good adhesive, stretching, swelling, self-healing, antibacterial, and antioxidant properties. *International Journal of Biological Macromolecules, 234*, Article 123718. https://doi.org/10.1016/j.ijbiomac.2023.123718

Talbott, H. E., Mascharak, S., Griffin, M., Wan, D. C., & Longaker, M. T. (2022). Wound healing, fibroblast heterogeneity, and fibrosis. *Cell Stem Cell, 29*(8), 1161–1180. https://doi.org/10.1016/j.stem.2022.07.006

Usme-Duque, L. K., Medina-Morales, M. A., León-Campos, M. I., Cruz-Requena, M., Ríos-González, L. J., Betancourt-Galindo, R., & Claudio-Rizo, J. A. (2026). Fermented plant extract-loaded collagen scaffolds: Bioactive hydrogels for enhanced wound repair and immune modulation. *Gels, 12*(2), Article 129. https://doi.org/10.3390/gels12020129

Wang, H., Yin, B., Sun, W., Geng, H., Wang, M., Li, Y., … Ni, N. (2024). CO_2-mediated alkali-neutralization curdlan hydrogels for potential wound healing application. *Biomacromolecules, 25*(3), 1738–1748. https://pubs.acs.org/doi https://doi.org/10.1021/acs.biomac.3c01233.

Wang, Z., Zheng, Y., Hu, Y., Yang, L., Liu, X., Zhao, R., … An, L. (2024). Improvement of antibacterial activity of polysaccharides via chemical modification: A review. *International Journal of Biological Macromolecules, 269*(Part 2), Article 132163. https://doi.org/10.1016/j.ijbiomac.2024.132163

Wojcik, M., Kazimierczak, P., Benko, A., Palka, K., Vivcharenko, V., & Przekora, A. (2021). Superabsorbent curdlan-based foam dressings with typical hydrocolloids properties for highly exuding wound management. *Materials Science and Engineering: C, 124*, Article 112068. https://doi.org/10.1016/j.msec.2021.112068

World Health Organization Newsroom. (2025). *Antimicrobial resistance*. https://www.who.int/news-room/fact-sheets/detail/antimicrobial-resistance.

Xia, G. X., Wu, Y. M., Bi, Y. F., Chen, K., Zhang, W.-W., Liu, S.-Q., … Liu, R.-H. (2021). Antimicrobial properties and application of polysaccharides and their derivatives. *Chinese Journal of Polymer Science, 39*, 133–146. https://doi.org/10.1007/s10118-021-2506-2

Xiang, C., Zhang, X., Zhang, J., Chen, W., Li, X., Wei, X., & Li, P. A. (2022). Porous hydrogel with high mechanical strength and biocompatibility for bone tissue engineering. *Journal of Functional Biomaterials, 13*, Article 140. https://doi.org/10.3390/jfb13030140

Xu, L., Wang, Y. Y., Huang, J., Chen, C. Y., Wang, Z. X., & Xie, H. (2020). Silver nanoparticles: Synthesis, medical applications and biosafety. *Theranostics, 10*(20), 8996–9031. https://doi.org/10.7150/thno.45413

Yang, X., Liu, Q., Chen, X., Yu, F., & Zhu, Z. (2008). Investigation of PVA/ws-chitosan hydrogels prepared by combined -irradiation and freeze-thawing. *Carbohydrate Polymers, 73*, 401–408. https://doi.org/10.1016/j.carbpol.2007.12.008

Zhang, Y., Zhang, Y., Jian, M., Pei, Y., Liu, J., Zheng, X., & Tang, K. (2024). Sustained-release, antibacterial, adhesive gelatin composite hydrogel with AgNPs double-capped with curdlan derivatives. *International Journal of Biological Macromolecules, 277*(2), Article 134222. https://doi.org/10.1016/j.ijbiomac.2024.134222

Zhangabay, Z., & Berillo, D. (2023). Antimicrobial and antioxidant activity of AgNPs stabilized with *Calendula officinalis* flower extract. *Results in Surfaces and Interfaces, 11*, Article 100109. https://doi.org/10.1016/j.rsurfi.2023.100109

Zhou, Z., Xiao, J., Guan, S., Geng, Z., Zhao, R., & Gao, B. (2022). A hydrogen-bonded antibacterial curdlan-tannic acid hydrogel with an antioxidant and hemostatic function for wound healing. *Carbohydrate Polymers, 285*, Article 119235. https://doi.org/10.1016/j.carbpol.2022.119235